CZECH TECHNICAL UNIVERSIT IN PRAGUE

FACULTY OF MECHANICAL ENGINEERING

Department of Production Machines and Equipment

Master’s Thesis

Control of the Robotic LMD-w Process for Achieving Desired Structural Sizes

Bc. Matouš Celba

2023 **1838**

MASTER'S THESIS ASSIGNMENT

I. Personal and study details

Student's name: **Celba Matouš** Personal ID number: **484040**

Faculty / Institute: **Faculty of Mechanical Engineering**

Department / Institute: **Department of Production Machines and Equipment**

Study program: **Robotics and Production Machines**

Specialisation: **Production Machines**

II. Master's thesis details

Master's thesis title in English:

Control of the Robotic LMD-w Process for Achieving Desired Structural Sizes

Master's thesis title in Czech:

Řízení robotického LMD-w procesu pro dosažení požadované velikosti struktur

Guidelines:

Scope of Work: The LMD-w process represents one of the standard AM (Additive Manufacturing) processes. One of the challenges in component production is the integration of laser source control, wire feeding, and robot path control to prevent material accumulation. Design, implementation, and practical validation of a control method for overlaying corrosion-resistant steel with feedback control. Thesis Outline:1. Technological characterization of the LMD-w technology. 2. Overview of control methods for the LMD process with feedback on trajectory, motion speed, wire feed rate, and laser power. 3. Familiarization with existing functions in control for laser robotic cell LASCAM. Proposal of a control strategy. 4. Design of samples with typical path entities to demonstrate the influence of feedback control. 5. Verification of results through sample creation and evaluation of their quality. Textual Content Length: 60 - 80 pages.

Bibliography / sources:

1) I. Gibson, D. Rosen, B. Stucker, and M. Khorasani, Additive Manufacturing Technologies. Cham: Springer International Publishing, 2021. doi: 10.1007/978-3-030-56127-7.
2) T. DebRoy et al., "Additive manufacturing of metallic components – Process, structure and properties," Progress in Materials Science, vol. 92, pp. 112–224, Mar. 2018, doi: 10.1016/j.pmatsci.2017.10.001.

Name and workplace of master's thesis supervisor:

Ing. Jan Brajer, Ph.D. Department of Production Machines and Equipment FME

Name and workplace of second master's thesis supervisor or consultant:

Ing. Martin Novák Department of Production Machines and Equipment FME

Date of master's thesis assignment: **13.10.2023** Deadline for master's thesis submission: **02.01.2024**

Assignment valid until: **15.09.2024**

Ing. Jan Brajer, Ph.D. Supervisor's signature	doc. Ing. Petr Kolář, Ph.D. Head of department's signature	doc. Ing. Miroslav Španiel, CSc. Dean's signature

III. Assignment receipt

The student acknowledges that the master's thesis is an individual work. The student must produce his thesis without the assistance of others, with the exception of provided consultations. Within the master's thesis, the author must state the names of consultants and include a list of references.

Date of assignment receipt	Student's signature

Declaration

I hereby declare that the presented thesis is my own work and that I have cited all sources of information in accordance with the Guideline for adhering to ethical principles when elaborating an academic final thesis.

I acknowledge that my thesis is subject to the rights and obligations stipulated by the Act No. 121/2000 Coll., the Copyright Act, as amended. I further declare that I have concluded a license agreement with the Czech Technical University in Prague on the utilization of this thesis as school work under the provisions of Article 60(1) of the Act. This fact shall not affect the provisions of Article 47b of the Act No. 111/1998 Coll., the Higher Education Act, as amended.

In Prague on January 2, 2024 ……..…….

Acknowledgments

I owe a special debt of gratitude to my thesis supervisor, Ing. Jan Brajer Ph.D., for his invaluable feedback and guidance, which were essential in the creation of this thesis. I would also like to express special thanks to my consultant, Ing. Martin Novák, who assisted me with experiment preparation and provided novel ideas for my work.

Finally, I wish to thank my family for their patience and support throughout my studies.

Annotation

Author:	Bc. Matouš Celba
Název DP:	Control of the Robotic LMD-wProcess for Achievieving Desired Structural Sizes
Extent:	78 pages
Academic year	2024
University:	ČVUT – Faculty of Mechanical Engineering
Department:	Ú12135 – Department of Production Machines and Equipment
Supervisor:	Ing. Jan Brajer Ph.D.
Consultant:	Ing. Martin Novák
Commissioner:	ČVUT – Facult of Mechanical Engineering
Field of use:	Process control to reduce postprocessing time and improving process stability
Key words:	Laser Metal Deposition, Additive Manufacturing, Closed-loop Control, Material Overfill in Corner Sections
Abstract:	This thesis explores the integration of closed-loop control in Laser Metal Deposition – wire (LMD-w) within Additive Manufacturing. It focuses on balancing material feed rate depending on the robot path and speed in order to minimize material overfill, particularly in sharp corners. The work includes a comprehensive overview of LMD-w technology and closed-loop control methods for LMD. The control strategy has been experimentally verified. This research is pivotal in enhancing the stability and reliability of the LMD-w process

Anotace

Autor:	Bc. Matouš Celba
Název DP:	Řízení robotického procesu LMD-w pro dosažení požadované velikosti struktur
Rozsah práce:	78 stran
Školní rok vyhotovení	2024
Škola:	ČVUT – Fakulta strojní
Ústav:	Ú12108.2 – Ústav výrobních strojů a mechanismů
Vedoucí magisterské DP:	Ing. Jan Brajer Ph.D.
Konzultant:	Ing. Martin Novák
Zadavatel:	ČVUT – FS
Využití:	Řízení procesu LMD-w pro zpřesnění výroby dílců a zredukování následného postprocessingu
Klíčová slova:	Laser Metal Deposition, Aditivní technologie, Zpětnovazební řízení, Akumulace materiálu v rozích
Abstrakt:	Tato práce se zabývá integrací zpětnovazebního řízení pro technologii LMD-w v rámci aditivní výroby. Praáve se zaměřuje se na regulaci rychlosti posuvu drátu v závislosti na dráze a rychlosti robota s cílem minimalizovat akumulaci materiálu v ostrých rozích. Práce obsahuje ucelený přehled o technologii LMD-w a zpětnovazebním řízením. Návrh řídící strategie byl experimentálně ověřen. Tento výzkum má zásadní význam pro zvýšení stability a spolehlivosti procesu LMD-w.

Contents

1 List of Abbrevations

AM	Additive Manufacturing
LMD-w	Laser Metal Deposition - wire
LMD	Laser Metal Deposition
PBF	Powder Bed Fusion
DED	Direct Energy Deposition
M/BJ	Material/Binder Jetting
L-PBF	Laser Powder Bed Fusion
E-PBF	Electron Beam Powder Bed Fusion
EBAM	Electron Beam Additive Manufacturing
WAAM	Wire-Arc Additive Manufacturing
LMD-p	Laser Metal Deposition with Powder
FGM	Functionally Graded Materials
GMAW	Gas Metal Arc Welding
GTAW	Gas Tungsten Arc Welding
PAW	Plasma Arc Welding
CMT	Cold Metal Transfer
GMAW	Gas Metal Arc Welding
GTAW	Gas Tungsten Arc Welding
PAW	Plasma Arc Welding
HAZ	Heat Affected Zone
CCD	Charge Couple Device
CMOS	Complementary Metal-Oxide-Semiconductor
IR	Infrared
CAM	Computer Assisted Manufacturing

OCT	Optical Coherence Tomography
PLC	Programmable Logic Controller
NC	Numeric Control
CAD	Computer Aided Design

2 List of Variables

Latin symbols

P	W	Laser power
v_t	$mm \cdot min^{-1}$	Traverse speed
v_w	$mm \cdot s^{-1}$	Wire speed
Δh	mm	Height increment
$\vec{v}_i$	$mm \cdot s^{-1}$	Velocity vector
$\vec{p}_i$	mm	Position vector
$\vec{t}$	s	Time vector
v_x	$mm \cdot s^{-1}$	Velocity in X direction
v_y	$mm \cdot s^{-1}$	Velocity in Y direction
$v_{t\_tracker}$	$mm \cdot s^{-1}$	Traverse speed from tracker
k	-	Sensitivity parameter
n	-	Number of layers
V	mm^3	Volume
d_w	mm	Wire diameter
L	mm	Length of deposition
t_d	s	Time delay in corners
ΔV	mm^3	Desired volume difference
v_{wr}	$mm \cdot s^{-1}$	Regulatory wire speed
i	-	Number of regulatory layers

3 Introduction

Additive Manufacturing (AM) stands at the forefront of a manufacturing revolution, offering unparalleled advantages in design flexibility, material efficiency, and the potential for manufacturing complex geometries with ease compared to traditional manufacturing methods. Among AM technologies, Laser Metal Deposition-wire (LMD-w) emerges as a particularly promising technique in manufacturing near-net shape parts, offering a fine compromise between dimensional resolution and build-up rate. However, the LMD-w process is demanding in terms of process stability. Without adept close-loop control, this technique faces risks of condition deviations or even failures during the process. The integration of closed-loop control is thus not just beneficial but essential in maintaining a stable process. Among all the present variables that were studied and attempted for close-loop control, managing overfill in sections with sharp corners has proven critical and still maintains being a deeply unexplored area of research. This focus is instrumental in advancing the stability, efficiency and reliability of the LMD-w process.

4 Objective

The objective of this thesis is to provide an overview and summarize the characteristics of various metal AM technologies, with a focus on the LMD-w technology. Furthermore, the theoretical section will review existing closed-loop control methods for the Laser Metal Deposition (LMD) process. The experimental part will investigate the process with regard to overfill formation. Subsequently, a close-loop control strategy including its validation will be proposed. An integrated control function will be also tested, and its functionality verified. This work also includes designing samples to demonstrate close-loop control effectiveness and verifying the results through quality checks of created samples.

5 Basic Concepts

In this chapter, the fundamentals of closed-loop control and its application for metal AM will be discussed. Initially, this chapter will introduce market-relevant metal AM technologies. Figure 5-1 illustrates that the Powder Bed Fusion (PBF), Direct Energy Deposition (DED), and Material/Binder Jetting (M/BJ) technologies are of highest market significance as of 2020 [1]. The focus will be on the LMD-w process and its advantages when compared to other methods.

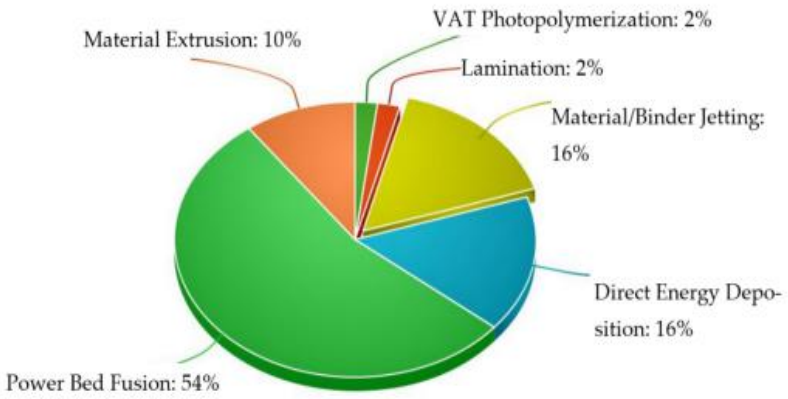

Figure 5-1: Metal Additive Manufacturing Market in 2020 [1]

The second part of this chapter will focus on the state-of-the-art closed-loop control in LMD. The content found in various research papers dedicated to this topic will be discussed and a comprehensive summary of the measured variables, employed sensors, controlled variables, and used and the desired effects adopted from the papers will be presented.

5.1. Powder Bed Fusion (PBF)

The majority of the metal AM market is represented by PBF technology (Figure 5-1). The basic working principle of this technique is that raw material in the form of powder is stored in a powder stock within the building chamber, from where it is usually delivered by a piston mechanism or gravity. Afterwards, the powder is evenly distributed onto the build platform by a leveling system, and any remaining powder is collected. The layer of powder particles is selectively fused by an energy source that melts the powder which then rapidly solidifies. The build platform is lowered after each layer and the process repeats itself until the desired part is manufactured.

The PBF machines use a laser beam (L-PBF) or an electron beam (E-PBF) as the energy source, with the laser being the more frequent one. [2] [3] Both sources have their respective advantages and drawbacks. The schematic depictions of these processes are in Figure 5-2. The L-PBF process is capable of higher feature resolution and a better surface finish than the E-PBF process. The electron beam requires a highly vacuumed chamber to function properly, while the L-BPF process requires a chamber flooded with inert gas to prevent oxidation. The scanning speed is much higher for the E-PBF, as it guides the electron beam through magnetic coils enabling almost instantenous beam movement In contrast, the laser beam is guided by gylvanometers, which have limited movement speed due to their inertia. [2] [4] The differences between L-PBF and E-PBF are summarized in Table 1.

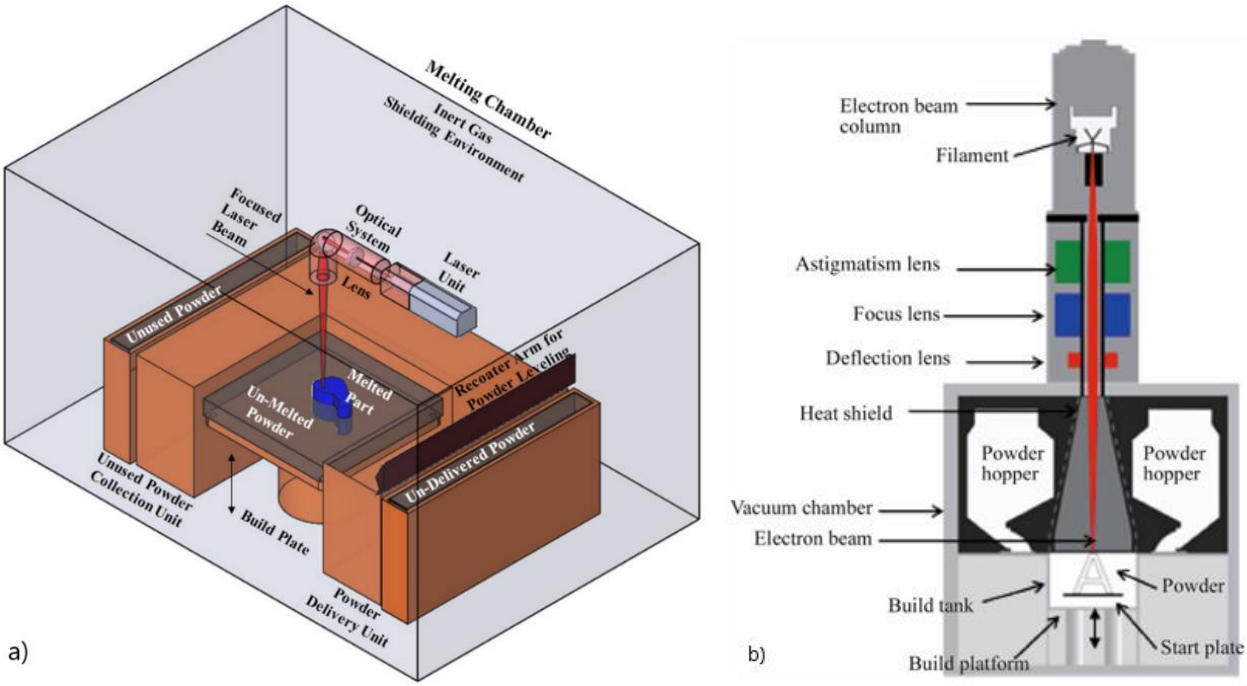

Figure 5-2 Schematic of the a) L-PBF and b) E-PBF process [5], [6]

PBF is a promising technology to manufacture high-performance metal parts with highly complex geometries. [3] One of the major benefits of the PBF process is its high precision and accuracy. The layer thicknesses for powder particle sizes ranging between 20 to 45 μm are in the range of 20 and 100 μm. [7] The dimensional accuracy falls within 0,04 to 0,2 mm. [8] However, PBF machines have relatively low build rates when compared to DED systems. Moreover, the dimensions of the building chamber limit the maximum size of manufacturable parts. Currently, the largest PBF machine has a building volume of 600 x 600 x 1500 mm [9], but much smaller build volumes are more common. [10]

Table 1 Differences between E-PBF and L-PBF [2]

Characteristic	E-PBF	L-PBF
Thermal source	Electron beam	Laser
Atmosphere	Vacuum	Inert gas
Scanning	Deflection coils	Galvanometers
Energy absorption	Conductivity-limited	Absorptivity-limited
Powder preheating	Use electron beam	Use infrared or resistive heaters
Scan speeds	Very fast, magnetically driven	Limited by galvanometer inertia
Energy costs	Moderate	High
Surface finish	Moderate to poor	Excellent to moderate
Feature resolution	Moderate	Excellent
Materials	Metals (conductors)	Polymers, metals, and ceramics
Powder particle size	Medium	fine

5.2.Direct energy deposition

DED processes work on the principle of using an energy source to melt the substrate and simultaneously melt the material fed into the place of deposition. The deposited material can be in the form of powder and the energy sources used for these processes are laser beam, electron beam, and electric arc. An important piece of hardware that usually integrates material feeding, energy source guiding and focusing, inert gas delivery and feed-back sensors is the deposition head [2]. The deposition head is usually mounted on a 6-axis robot arm or 5-axis CNC to enable the production of complex parts [11] [12] [13] [14] [15] [16]. The deposition rate of the DED processes is greater than that of PBF processes, on the other hand, the minimum layer thickness, the surface roughness, and the minimum feature size are smaller for PBF fabricated parts [16]. Processes that fall under DED are LMD, Electron Beam Additive Manufacturing (EBAM), and Wire and Arc Additive Manufacturing (WAAM).

5.3.Laser metal deposition with powder

The most common DED process is the laser metal deposition process with powder (LMD-p). [2] The deposition principle of this method is based on feeding metallic powder into the melt pool created on the substrate by a laser beam. The powder is fed by inert gas through one or multiple nozzles attached to the deposition head, which can be either coaxial or off-axis to the laser beam [8]. Coaxial powder feed is schematically depicted in Figure 5-3. The main benefit of the off-axis nozzle is the simplicity of design, which also means lower costs. The off-axis feeding is often employed for outside diameter overlaying of cylindrical sections, or hard-to-get places for coaxial powder feed such as grooves and channel's inner diameters. The main disadvantage of the off-axis nozzle is that the process conditions are direction-dependent. To have a consistent shape of deposition, the relative movement of the deposition head to the substrate must be unidirectional [17]. Coaxial nozzles are more widely used for the LMD-p process, as they enable consistent omnidirectional deposition, higher capture efficiency of powder, and accuracy compared to the off-axis nozzle [17] [18]. By separately controlling the powder feed rate of different materials, the production of Functionally Graded Materials (FGM) can be achieved [18].

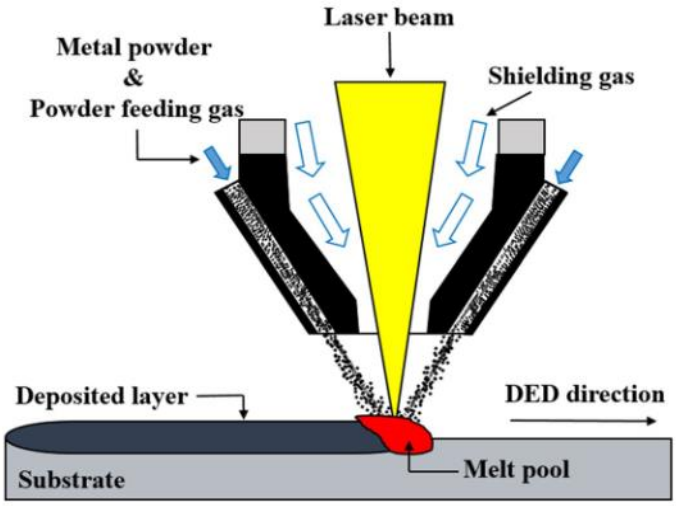

Figure 5-3: Schematic of the LMD-p process [19]

The advantage of LMD-p when compared to other DED processes is the relative ease of matching the powder with a shaped laser beam, such as Tophat. There are also more available alloys in the form of powder than in wire [20]. The dimensional accuracy of LMD-p is also supreme to the wire-based processes [16],[21]. However, the use of powder also has its

drawbacks, one of them being high material losses. The capture efficiency of powder is under 90% [22], whereas wire utilization is nearly 100%, except for splatter. Furthermore, powder has typically lower material purity and is more susceptible to contamination during the process due to its larger surface area when compared to the same volume of wire [23]. Moreover, powder materials are more expensive than wired materials [24].

5.4.Electron Beam Additive Manufacturing

Similarly to the LMD process, EBAM utilizes an electron beam as the energy source to create a melt pool on the substrate into where the feedstock material is fed. As for the E-PBF process, EBAM requires a high vacuum working environment to prevent electron scattering by the collision of electrons and molecules of air [25]. Due to the difficulty of powder feeding in a vacuum and the ionization of carrier gas, wire feedstock is employed [26]. The process is illustrated in Figure 5-4.

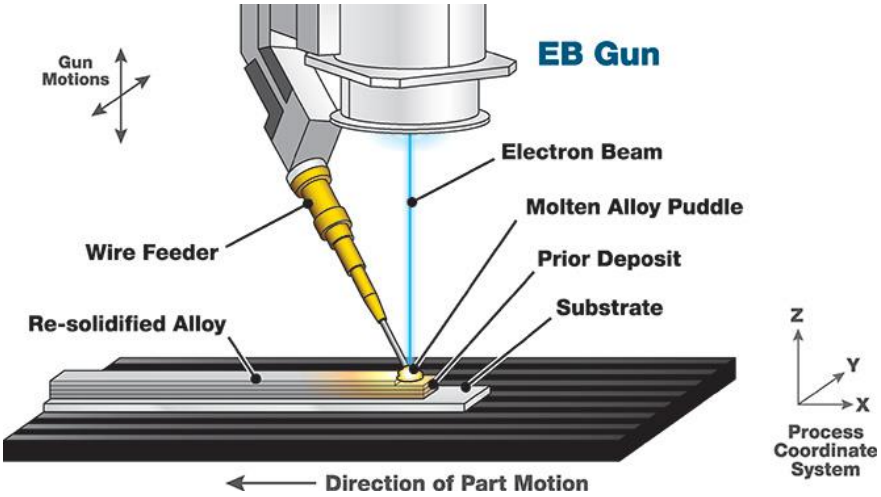

Figure 5-4: Schematic of the EBAM process [27]

Wire-feed AM processes have higher deposition rates in contrast to powder-based AM [28]. EBAM has demonstrated the highest deposition rate among the DED processes (330g/min for stainless steel), thus being suitable for the production of large-volume parts [29]. Electron beam-based processes offer added advantages over laser-based processes, including higher power efficiency, and the ability to process highly reflective materials such as copper, aluminium, and titanium effectively [25],[29],[30]. Furthermore, the cost of an electron beam source is generally lower compared to that of a laser source. While the high vacuum environment not only ensures the quality of the electron beam but also effectively prevents

material oxidation, it is important to mention that the process of evacuating the building chamber is time-consuming. Depending on the chamber's size, evacuation can take approximately 30-40 minutes, or even longer [25].

5.5. Wire and Arc Additive Manufacturing

The WAAM technology employs an electric or plasma arc to melt the feedstock wire, thus depositing it onto the substrate. The process can be distinguished into three different variants based on the heat source. These different types are namely Gas Metal Arc Welding (GMAW), Gas Tungsten Arc Welding (GTAW), and Plasma Arc Welding (PAW) [31]. The GMAW process has a 2-3 times higher deposition rate than that of GTAW or PAW methods [32]. For the GMAW-based WAAM, the arc is established between the tip of the consumable electrode serving as feedstock material and the substrate. The electrode is fed coaxially, resulting in omnidirectional deposition symmetry [16]. GTAW and PAW both use a non-consumable tungsten electrode to establish an arc. These two technologies suffer from the off-axis feeding of material, thus being sensitive to arc length and direction of deposition [33]. However, GTAW- and PAW-based WAAM have been demonstrated to be more stable processes with less spatter, weld fume, excessive heating, distortion, and porosity when compared to GMAW [32],[33]. A modified GMAW variant, Cold Metal Transfer (CMT), based on controlled dip transference, can be implemented to lower the heat input, stabilize the arc and create a spatter-free transference [33]. The WAAM process is illustrated in Figure 5-5.

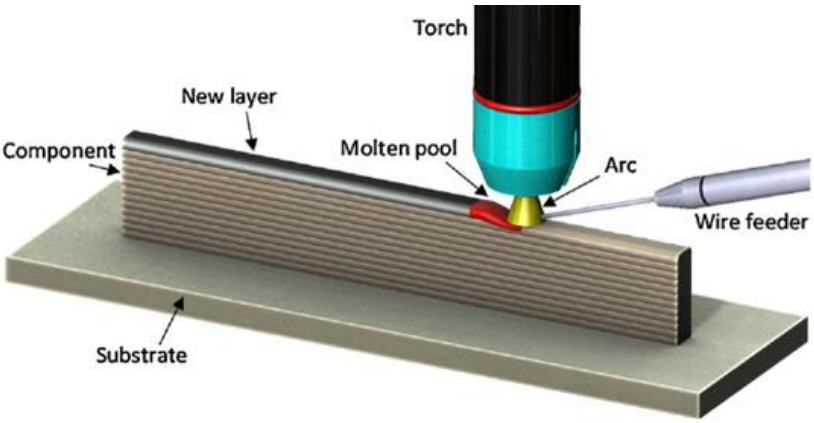

Figure 5-5: Schematic of the WAAM process [34]

The equipment needed for WAAM is less expensive than that for EBAM and LMD, thus providing a cost-effective alternative for the production of AM parts [35]. WAAM also has relatively high deposition rates within the range of 16,7-66,7 g/min [16]. However, the process lacks precision and the high heat input from the arc causes significant distortions and residual stress. [36]

5.6.Laser Metal Deposition with Wire

In principle, LMD-w is similar to LMD-p, with the primary difference being the use of wire as feedstock material. The laser beam creates a melt pool on the substrate, into which the wire is fed and melted. The wire can either be fed coaxially or off-axis as is shown in Figure 5-6, with both approaches having their already above-mentioned advantages and limitations. LMD-w is a versatile process combining the benefits of the other DED processes. When compared to the LMD-p process, LMD-w offers several advantages such as higher deposition rates (1,5 - 48 g/min), increased material efficiency, improved surface roughness, and a safer working environment for operators [16],[28]. Furthermore, LMD-w does not require the time-consuming and expensive evacuation of the building chamber and it offers more geometrical integrity than WAAM [37]. Moreover, the heat input is not as big as with the WAAM process, resulting in smaller distortions and residual stresses [38].

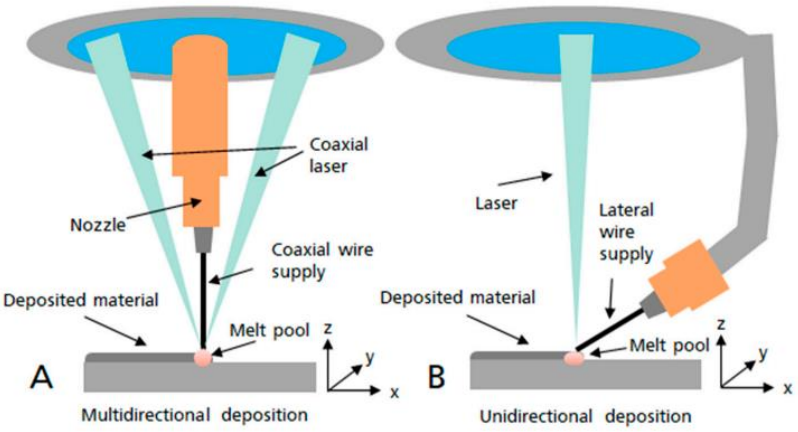

Figure 5-6 Schematic of the LMD-w process with A – coaxial wire feed, B – off-axis wire feed [39]

The off-axis wire feeding is a more commonly employed solution, as for the coaxial wire feeding a much more sophisticated deposition head with complex optics is required [16]. Such deposition heads are available on the market, with each one taking a different approach to the problem.

A German company developed the CoaxPrinter deposition head, which uses shaping lenses and splitting beams to align the laser beam with the wire. The beam is first shaped into a ring and then split in half so the wire can be introduced without interfering with the laser beam. The beam is then brought back into the form of a ring and is focused on the output of the deposition head by a focusing lens [40]. This deposition head and schematic of the optics is shown in Figure 5-7.

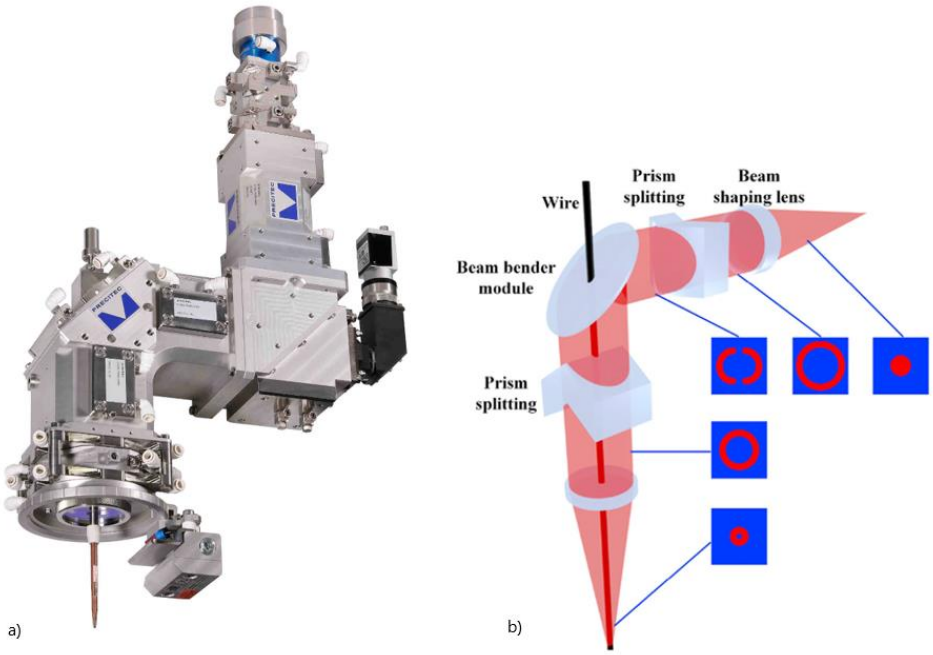

Figure 5-7: a) Coaxprinter deposition head, b) Schematic of the beam handling optics of CoaxPrinter [40], [41]

The Fraunhofer IWS research center designed the COAXwire and COAXwire mini deposition heads. The collimated laser beam is divided into three separate beams by optics. The beams are subsequently focused onto a circular focal point. A schematic of the three-beam laser is illustrated in Figure 5-8.

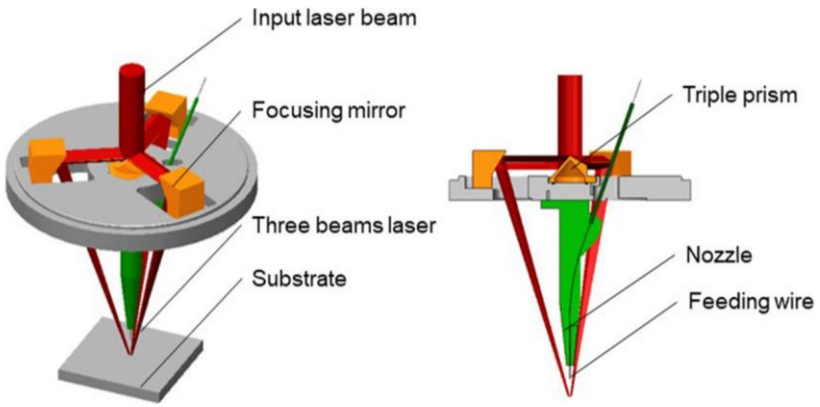

Figure 5-8: Schematic of a three-beam laser with coaxial wire feeding [42]

Wires of 0,4 to 1,6 mm in diameter can be used by the COAXwire [43], while COAXwire mini can use finer wires with a diameter of 0,1 to 0,6 mm to produce filigree structures. [44] The COAXwire deposition head mounted on an industrial robot is shown in Figure 5-9.

Figure 5-9: COAXwire deposition head [43]

A highly compact LMD-w system was developed by a Spanish 3D printing company Meltio. The deposition head implemented in the printer uses six diode lasers guided through fiber optics into a collimator mounted coaxially to the laser head [45]. The maximum output of the deposition head is 1200 W and wires from 0,8 to 1,2 mm in diameter can be used [46].

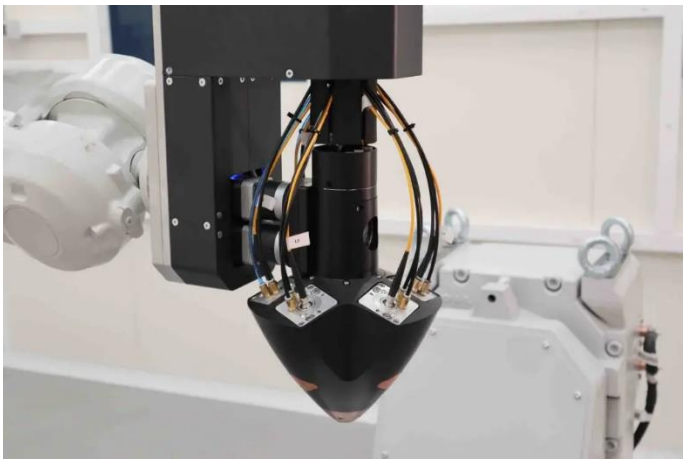

Figure 5-10 Meltio deposition head [47]

The constant mechanical connection between the deposition head and the substrate via wire introduces specific defects known as “dripping” and “stubbing”. The dripping defect occurs when excessive energy is introduced into the process, while stubbing is the result of insufficient energy input. Moreover, precise alignment of the laser focus and wire is crucial for the stability of coaxial wire feeding [48].

5.7. Additive manufacturing technologies summary and comparison

In previous chapters, the working principles of various processes from the category of PBF and DED were described. This chapter will provide a clear summary of the merits and limitations that characterize AM technologies.

The deposition rate of the DED processes is higher than that of the PBF processes, while the minimum layer thickness and feature size are in favor of PBF [16]. Furthermore, wire-feed DED processes, such as EBAM, WAAM, and LMD-w have superior deposition rates to those of powder-feed technologies. Figure 5-11 shows that there is a trade-off between high deposition rate and high resolution.

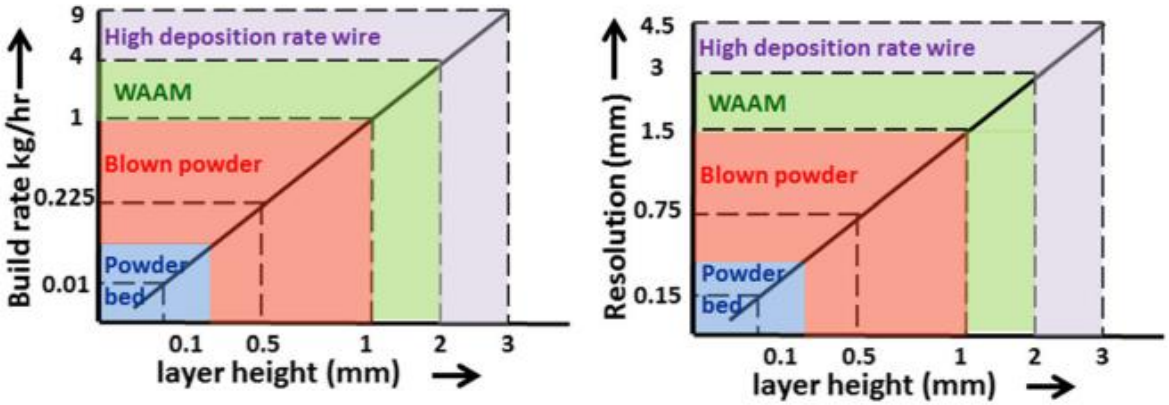

Figure 5-11 AM technologies and their build rate and resolution dependency on layer height [28]

The surface accuracy is majorly influenced by the layer thickness of the deposited layer, thus by the use of additive technology. The surfaces of parts are approximated by layer upon layer, with each layer having a certain layer thickness. This effect is called “stair stepping” and it is illustrated in Figure 5-12 [49].

With increasing layer thickness, the dimension error normal to the deposition direction also increases, thus meaning that processes with lower layer thicknesses such as PBF and LMD-p have higher surface accuracy and need less post-processing in contrast to wire-feed technologies [50].

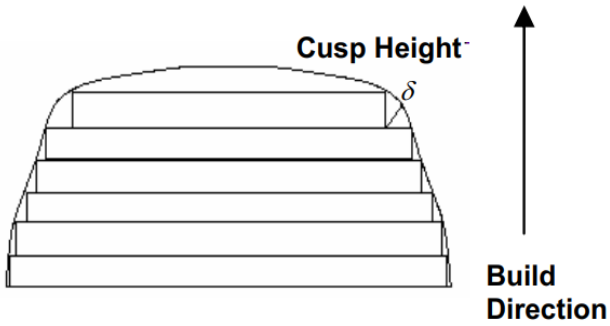

Figure 5-12 The illustration of the „stair stepping“ effect [50]

Table 2 gives an overview of the AM technologies and their characteristics such as feedstock material, energy source, deposition rate, layer thickness, dimensional accuracy, and surface roughness.

Table 2 – Comparison of AM technologies

Process	Material	Energy source	Deposition rate [g/min]	Layer thickness [µm]	Dimensional accuracy [mm]	Surface roughness [µm]	References
L-PBF		Laser	N/A	10-100	0,04 – 0,2	5 - 20	[8], [21]
E-PBF	powder	Electron Beam	N/A	50-200	0,05 – 0,2	7 - 20[21]	[8], [21], [51]
LMD-p		Laser	<10	50-500	0,5 – 1	4 - 10[21]	[2], [16], [21], [28]
EBAM		Electron Beam	<330	<3000	1 – 1,5	8 - 15	[8], [21], [28]
WAAM	wire	Electric/Plasma Arc	12-66,7	1000-2000	±0,2	200	[16], [28]
LMD-w		Laser	1.5-48	>1000	±1.5	40-60	[16] [52]

6 Closed-loop control of LMD

In LMD, the quality and stability of the process are influenced by the main processing variables such as material feed rate, laser power, traverse speed, layer thickness, and step-over value. It is crucial to optimize and fine-tune these parameters prior to the process to ensure a consistent and stable outcome. However, the presence of disturbances such as changes in thermal conditions (often transitioning from 3D to 2D conduction during the process) or small variations in variables like thermal conductivity (a material property dependent on temperature), traverse speed (the speed decreases in sharp corners), or laser power necessitates the implementation of an in situ monitoring and control system [53].

Despite its major benefits, coaxial wire feeding's high sensitivity towards disturbances poses a major challenge to the stability of the process. To prevent “stubbing” and “dripping” during the process, real-time monitoring and control of the variables are required [54]. The following chapters discuss which variables are monitored and controlled in closed-loop control of the LMD process and the related sensors.

6.1. Melt pool temperature control

Melt-pool temperature is an important variable that influences the quality of the deposition [55]. Studies have shown that using fixed process parameters, meaning constant laser power – P [W], constant traverse speed v_t [mm/s], and constant material feed throughout the deposition, will cause an increase in the temperature of the substrate with progressing deposition [56]. The heat affected zone (HAZ), dilution, and residual stress increase with the rising temperature [56] [57]. The increasing temperature of the substrate also causes the “mushroom effect”, which is the width increase of beads in a multilayer vertical deposition [58]. All these effects are caused by unregulated heat input, while conditions such as substrate temperature and thermal conductivity change, and have a negative influence on the quality of deposition [55]. Therefore, the temperature control of the melt pool is of great importance to the quality of deposition. Notably, the literature indicates that laser power has the highest influence on melt-pool temperature [59].

6.1.1. Sensors for melt pool temperature measurement

While the most common way to measure the temperature of an object is through heat conduction between the object and a heat-sensitive element [60], this approach is not possible for measuring melt-pool temperature during the LMD process. For melt-pool temperature

measurements, non-contact thermometers are used. One of the most incorporated sensors for temperature measurement is the pyrometer. Pyrometers allow an easy non-contact temperature measurement as they evaluate temperature with the use of Plank's radiation law, where an object generates visible radiation of certain wavelengths, depending on the measured material, size of the measured object, and also the distance and viewing angle of the pyrometer relatively to the measured object [61],[62]. The two basic types of pyrometers are optical pyrometers and radiation pyrometers, which differ in the temperature ranges they measure. Most materials used for LMD have a higher melt pool temperature than n 800 °C, falling into the ranges of optical pyrometers. [56], [60]. The available literature confirms their feasibility for applications to closed-loop control of melt-pool temperature [54], [56], [63]. While other sensors used for melt-pool temperature measurements, such as Charge Couple Device (CCD) [64], Complementary Metal-Oxide-Semiconductor (CMOS) cameras [65], or Infrared (IR) cameras [66] require additional data handling to acquire the temperature signal, pyrometers provide the signal directly. Application of photodiodes [67] can also be found that fall into the same category as pyrometers in terms of the sensing signal [68].

While IR cameras are set to sense infrared signals, CCD and CMOS cameras can sense both the visible and infrared spectrum. Signals in the infrared spectrum are more accurate in calculating temperature data, as the visible spectrum can be disturbed by different layer colors and other process phenomena. The advantages of CCD and CMOS cameras over IR cameras are their low costs, high resolution, and high frame rate. However, they require filters to eliminate the visible spectrum and are overall poor in temperature monitoring compared to the IR cameras. IR cameras are more costly, but their ability to a wide range of temperature monitoring is supreme thanks to different types of different sensing wavelengths. [68]

6.2.Melt pool geometry characteristics control

Although temperature control can majorly improve the quality of deposition, it cannot ensure a uniform track morphology in multilayer deposition. It has been observed that even with controlled temperature, the bead geometry changes as the deposition progresses [56]. This is because the uniformity of the deposition relies on the melt pool size consistency [55]. Controlling the melt pool width [53], [69]–[72] together with height [73] or both [74], can improve the geometric accuracy and maintain consistent process conditions.

6.2.1. Sensors for melt pool geometry characteristics measurement

The measurement of melt pool geometry characteristics mainly relies on camera sensors, such as CMOS and CCD cameras [53], [69], [71]- [73]. The cameras usually have a high frame rate of around hundreds of Hz [75], that capture images of the melt pool that are then evaluated by computing software. The melt pool geometry is measured automatically through the binarization of the images. The next step is to evaluate the binarized data to acquire the geometry characteristics. The process is described in Figure 6-1. Some approaches also implemented image processing from IR cameras [70].

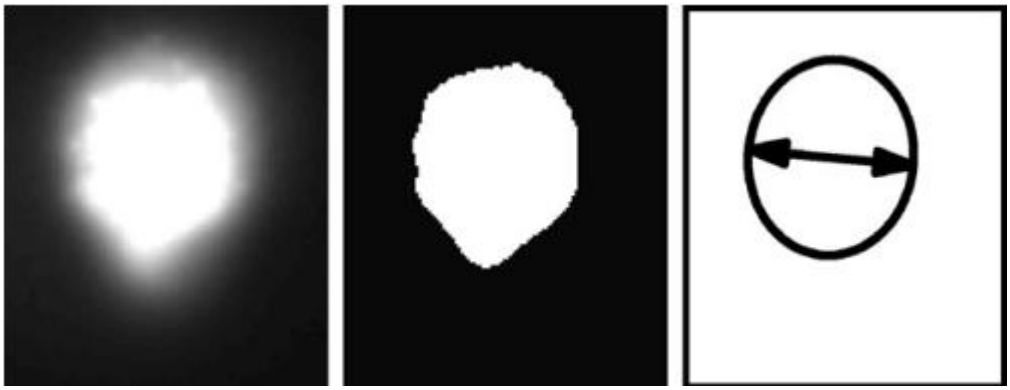

Figure 6-1: Left: original image from camera; Center: binarized and filtered image; Right: fitted ellipse for measurement [76]

6.3. Over-deposition and height control

While LMD incorporates a highly focused energy source and is thus able to produce near-net shape parts [37], the process suffers from over-deposition in sharp corners, affecting the structural integrity during the build-up. One reason for material accumulation is the slowed movement of the deposition head in corner sections. This happens due to the motion controller's need to change the speed vector direction, thus decelerating in the current movement direction and reaccelerating in the new path direction after the corner. With constant process parameters, mainly material feed, the time difference in passing the corner section with decreased speed compared to the straight sections leads to excess material deposition [77]. The second factor influencing the over-deposition is the overlapping of beads determined by the trajectory of the deposition head. The volume of excess material due to the overlapping depends on the angle of the corner and the bead geometry. The geometry of the beads for LMD-w is dependent on the process parameters, namely traverse speed, wire feed rate, and laser power [78]. Figure 6-2 shows the overlapping zone of two beads deposited on a path with a sharp angle.

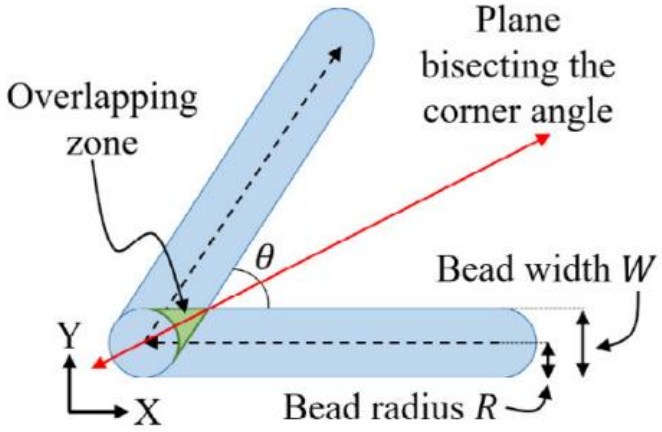

Figure 6-2 Illustrated area of overfill Ao due to overlapping beads at a corner section [79]

Strategies to prevent overfill in sharp corner sections can be found in the literature, mostly for LMD-p. One documented approach is to artificially increase the radius of the deposition path from 0 mm (sharp corners) to create rounded corners. This achieves higher consistency in the traverse speed of the deposition system and also reduces the overlapping area of the beads [77], [80]. However, design freedom is sacrificed as sharp corners cannot be manufactured and precision is compromised. Another approach is to create geometric models to predict the deposition geometry and modify the process before the actual deposition according to the results. Analytical [81], numerical [79], and models based on artificial intelligence [82] have been developed for the LMD-w process, however, they are limited by the number of different deposition geometries, combinations of process parameters that influence bead geometry, and other disturbances. To increase the robustness of the LMD-w process regarding geometrical precision and stability, closed-loop control strategies are necessary.

Traverse speed and material feed rate are the most influential process parameters influencing bead height [78], [83], thus strategies to mitigate overfill at the corner section by altering these parameters were also explored. Woo. et al. [84] stated that for LMD-p the material feed rate is the dominant parameter determining the height of deposition, however, the delayed feedback of the material feed system limits the control of the feed rate in real-time. Therefore, traverse speed modifications at the corner sections of the deposition were incorporated by [79] [84] to compensate for the overfill in the LMD-p process. Due to the already mentioned delay of regular feeder systems, a novel powder flux regulation system was designed by Arrizubieta et al. [85] that could instantaneously control the mass flow rate and its implementation reduced the overfill at corner sections. However, these solutions do not contain closed-loop control.

Closed-loop control of deposition height was implemented by [86], [87] using a CCD camera to monitor the height of the deposition and regulate the traverse speed of the deposition head on geometries without sharp corners for the LMD-p process. Hua and Choi [88] attempted to control the deposition height by measuring the height with 2 optical distance sensors and regulating the laser power. The laser power has a direct effect on material catchment efficiency and, thus on the bead geometry. However, this effect does not occur for wire-based LMD. Studies on closed-loop deposition height control of the LMD-w process can also be found. Heralić et al. [89] measured the layer height with a laser line scanner and manipulated the wire feed rate. Unlike the LMD-p powder feed rate, the wire speed can be controlled with minimal delay, giving an advantage over the powder-based LMD process. Different work by Garmendia et al. [37] proposed the use of a structured light scanner to measure the height of a multilayered deposition and modify the deposition trajectory in Computer Aided Manufacturing (CAM) based on the remaining volume to be deposited. Another control strategy developed by Takushima et al. [90] used a laser line beam and a camera for the height measurement while regulating the wire speed linearly based on the measured height. Bernauer et al. [91] controlled the deposition height through wire speed and segmentation height measurements using a laser line scanner and a CMOS camera. A novel approach using a MISO controller was developed by Song et al. [92], where a height master controller blocked the slave temperature controller if over-building was detected by CMOS cameras, and became transparent when the height was below the prescribed value. The slave temperature controller then regulated the laser power to increase the powder catchment of the melt pool. Tang and Landers [93] used a layer-to-layer height control by adjusting the powder feed rate between layer deposition based on the height measurement of the previous layer. Finally, an Optical Coherence Tomography (OCT) sensor was used for the height measurements by Becker et al. [94] also controlling the wire feed rate to maintain constant deposition height. Although not using closed-loop control of the deposition height, Heralić et al. [95] implemented a feed-forward compensator, to measure the height of previously deposited layers and compensate for the irregularities of the previous layers.

In conclusion, the control methods and approaches for powder and wire-based LMD processes differ due to the characteristics of the processes. LMD-p suffers from the material feed response delay, thus strategies with traverse speed control are frequently used. However, traverse speed control for overfills in corner sections can only be achieved by highly dynamic CNC systems and is not suitable for robotic manipulators due to acceleration limits in joints [96] as cited in

[81]. For a robotic LMD-w process, the wire feed rate is a more feasible controlled variable for achieving desired structural sizes.

6.3.1. Sensors for overfill and height deposition measurement

For overfill and height measurement, the already mentioned CCD and CMOS cameras also found their field of application. Furthermore, laser displacement sensors and laser line scanners based on triangulation have also found their use in height measurement in LMD systems [89], [91], [93]. Another emerging approach from is-situ height measurement is the OCT sensor. The OCT sensor consists of a light source emitting a beam of light with low coherence length and a Michelson interferometer. The beam is split into a measurement and reference path by a beam splitter, where the measured object is irradiated by the beam in the measurement path. A part of the beam is reflected back into the beam splitter, where it combines itself with the beam from the reference path and follows the path to the detector. The detector will then evaluate the distance based on the interference signal. [97] An OCT sensor is illustrated in Figure 6-3.

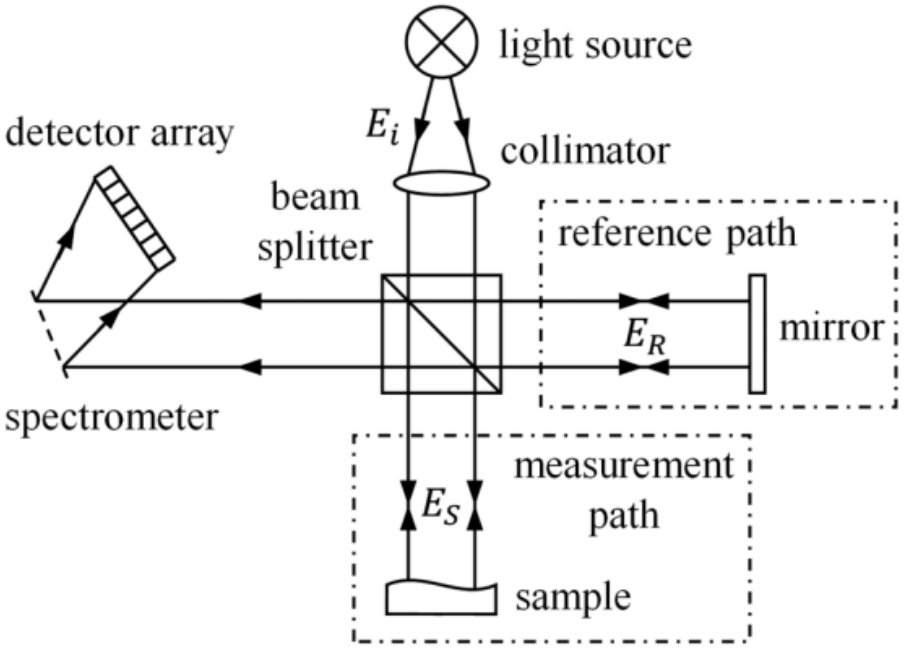

Figure 6-3: Schematic of an OCT sensor [98]

6.4. Closed-loop control summary

Closed-loop control in LMD focuses on regulating main process variables such as laser power, material feed rate, and traverse speed to ensure process stability and consistency. Among the main variables implemented in closed-loop control is the melt pool temperature, which has a major influence on the quality of the deposited parts. Sensors like pyrometers, photodiodes, IR, CCD, and CMOS cameras are used for temperature measurement. Laser power, having the highest influence on the melt pool temperature, is, therefore, the regulated variable in existing closed-loop control approaches.

By controlling melt pool geometry characteristics, the uniformity of bead morphology is improved. Melt pool width and height are primarily monitored by CMOS and CCD sensors, which provide high frame rate images of the melt pool during the deposition. After processing the images, the system can automatically evaluate the geometry characteristics and regulate the corresponding process parameters. Since the melt pool geometry is related to the melt pool temperature, the regulated process parameter is also laser power.

To avoid over-deposition and maintain structural integrity, it is necessary to monitor the height of the deposition during the process. Methods using CCD and CMOS cameras were by some research groups, whereas others developed monitoring systems using triangulation sensors or OCT sensors. Different regulation approaches are available, some control the material feed rate, and some laser power (suitable only for LMD-p) or traverse speed.

Each control method employs specific sensors a varies in its control strategy, determined by the regulated process parameter or used controllers. Apart from the above-mentioned control strategies, there are also unique closed-loop control approaches attempting to indirectly control microstructure properties [66] or dilution [76]. The reviewed literature on closed-loop control of LMD is summarized in Table 3.

Table 3: Summarized literature review on closed-loop control of LMD

Controlled variables	Measured variables (Input)	Sensor	Regulated variable (Output)	Controller	Reference
Melt pool temp.	Melt pool temp.	Ge Photodiode	Laser power	PID controller	[67]
					[56]
		Pyrometer		PI controller	[54]
				N/A	[99]
				PSO controller	[55], [58]
Melt pool width	Melt pool width	CMOS camera	Laser power	PI controller	[53], [71]
				PSO-LQR	[69]
		IR camera		N/A	[70]
		CCD camera		PC	[72]
Melt pool height	Melt pool height	CCD camera	Laser pulse energy	PID controller	[73]
Deposition height	Deposition height	CCD Camera	Traverse speed	PID Controller	[86]
				PI controllers	[87]
		Optical height sensors	Laser power	Fuzzy controller	[88]
		Laser line scanner		ILC controller	[89]
		Camera		N/A	[90]
		Laser line scanner, CMOS camera	Wire feed rate	Matlab	[91]
		OCT sensor		PI controller	[94]
		IR camera, Laser displ. sensor	Powder flow	PSO Controller	[93]
	Melt pool height, Melt pool temp.	CCD camera, Pyrometer	Laser power	MISO controller	[92]
Melt pool width, Melt pool height	Melt pool width, Melt pool height	CMOS Camera, OCT sensor	Laser power, Traverse speed	PI, PID, LQG controller	[74]
Melt pool width, Bead height	Melt pool width, Layer height	Camera, laser displ. sensor	Laser power, wire feed rate	PI controller, feed-forward compensator	[95]
Height increment	Deposition height	Structured light scanner	CAM data	N/A	[37]
Microstructure properties	Melt pool temp.,	IR Camera, CCD Camera	Traveling speed	PID controller	[66]
Dilution	Melt pool width	CMOS camera	Laser power	PI controller	[76]

7 System, Materials, and Methods

7.1. Laser Metal Deposition System

The used LMD-w system consists of a deposition head, an industrial robot, a wire feeding unit, and a safety chamber. The main component, the coaxial deposition head (CoaxPrinter, Precitec GmbH & Co. KG, Gaggenau, Germany), is stored alongside other laser heads with different technologies within the safety cabin and is manipulated by a 6-axis industrial robot (KR-60, KUKA AG, Augsburg, Germany) with a maximum load capacity of 60 kg and radial workspace of 2m. The kinematic possibilities of the system are enhanced by a linear axis of the robot to increase workspace size and by a 2-axis tilting table (KP2-HV500, KUKA AG, Augsburg, Germany). As described in Chapter 5.6, the head features a unique ring-shaping optical system that evenly distributes the energy. The optics are shielded from spatter and other impurities generated during the process by a cross jet and shielding glass. Moreover, argon is directly delivered into the process by a nozzle to prevent oxidation.

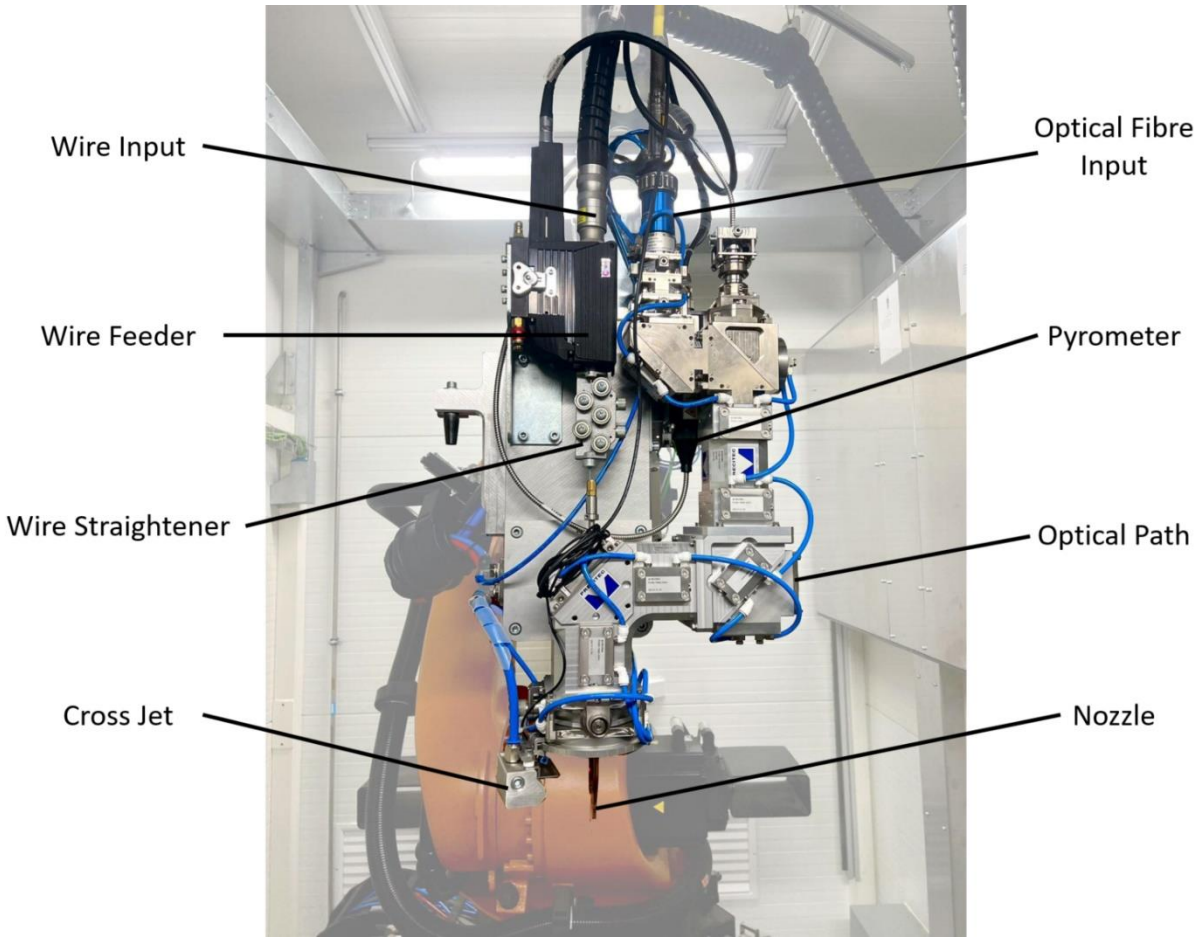

Figure 7-1: CoaxPrinter deposition Head mounted on KUKA KR-60

A 6 kW laser source (YLS 6000, IPG Photonics, Marlborough, USA) was used to generate a continuous laser beam with a wavelength of 1070 nm. The wire is being delivered by a wire feeding unit (MFS-V3, Alexander Binzel Schweisstechnik GmbH & Co. KG, Buseck, Germany) able to deliver wire of 0.8 – 1.6 mm in diameter.

For safety reasons, the unit contains multiple safety measures, such as a safety chamber with sensors, that will automatically shut down the system if they are damaged. Additionally, the safety chamber is constructed out of durable material, designed to withstand the laser beam for a short amount of time to give the operator time to press a total stop button. There are multiple total stop buttons around the system and there is also a safety lock on the door of the safety chamber. The safety needs to be checked before starting the process, without it the control system won't start any NC program. The control system is Sinumeric 840D from Siemens and it is responsible for the movement of the robot, other processes such as laser, process gas feeding, and wire feeding are controlled through a programmable logic controller (PLC).

For the measurement of height and overfill a structured light 3D scanner was used. (GOM ATOS Capsule, Carl Zeiss GOM Metrology GmbH, Braunschweig, Germany). The scanner can be operated in an automatic, semi-automatic, or manual setting. In the automatic setting, the scanner is mounted on a robotic arm, while with the semi-automatic setting, it is mounted on a 3-axis system with a Z-axis and a tilt-rotating table. In the manual setting, the operator uses a stand and manually positions the scanner relative to the scanned part. The scanner was calibrated before the measurement for optics with a measuring area of 320 x 240 mm. According to the calibration list, the scanner's precision is stated as 0,01 mm. Figure 7-2 shows the scanner with a calibration raster during the calibration process.

Position data of the robot were obtained from the control system by using the trace function. The data were positions from encoders and to verify them, they were compared to data from a laser tracker (Leica Absolute Tracker AT960, Leica Geosystems AG, Heerbrugg, Switzerland). The typical values for distance accuracy are ± 5 μm, ± 7.5 μm + 3 μm/m for angular accuracy, and ± 0.2 μm + 0.15 μm/m for interferometer accuracy.

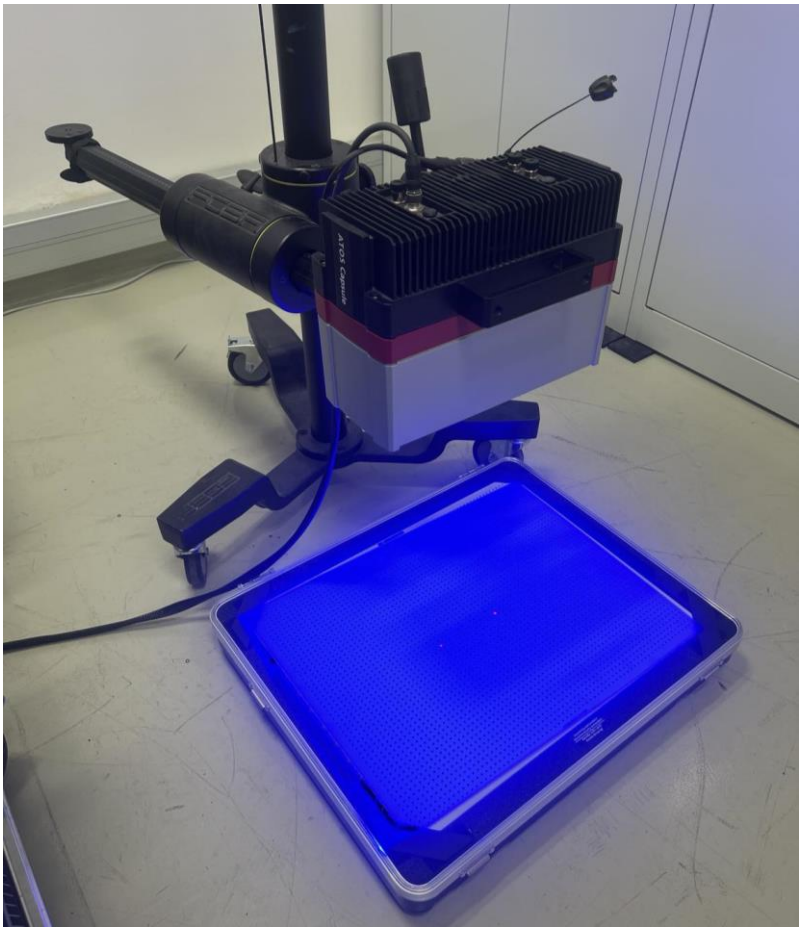

Figure 7-2: Calibration of the 3D scanner GOM ATOS Capsule

7.2.Materials

For the experiments, a plate from AISI 304 alloy, measuring 110 x 110 x 12 mm^3, was used as a substrate. The substrate was fastened to the rotating table at 4 corners to reduce thermal distortions. The wire fed into the process was the OK Autrod 316LSi, manufactured by ESAB with a diameter of 1.2 mm. The typical chemical composition of this alloy is detailed in Table 4.

Table 4: Typical chemical composition in % of OK Autrod 316LSi wire and AISI 304 alloy [100] [101]

Wire	C	Mn	Si	Ni	Cr	Mo	Cu	Ferrite
	0.01	1.8	0.9	12	18.4	2.6	0.12	7
Substrate	C	Mn	Si	Ni	Cr	P	S	N
	0.07	2.00	1.00	8.0-10.5	17.5-19.5	0.045	0.03	0.1

7.3.Methods

The primary objective of this work is to mitigate overfill in sharp corners due to the overlapping of the beads and deceleration of the deposition head. To test the effect of different angles on the amount of overfill material, a part including five distinct angles was specifically designed for the experiment. The design of this part, including the starting point and direction of the deposition is illustrated in Figure 7-3.

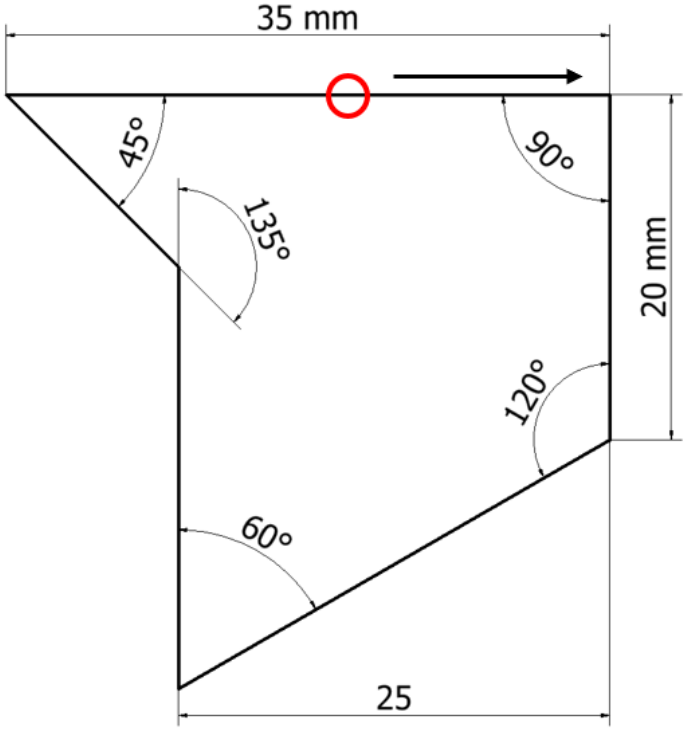

Figure 7-3: Design of experimental part

The Numerical Control (NC) code for the system is generated by a postprocessor integrated into CAM Siemens NX. The geometry of the desired part and substrate needs to be input into the CAM interface together with process parameters for the LMD-w process. The main process parameters of LMD-w include laser power P [W], traverse speed of the deposition head v_t [mm·min^{-1}], wire speed v_w [mm·s^{-1}], and the height increment between layers Δh [mm]. The process window for LMD-w using the same deposition head and stainless steel was identified by Zapata et al. [78]. However, process parameters were taken from Novák [102], where he studied the process parameters of the same system and found a set of parameters that produce quality, defect-free depositions. The parameters identified in this study align with the process window from Zapata et al., and thus have been selected for use in this work.

Table 5: Process parameters for LMD-w

P [W]	v_t [mm·min^{-1}]	v_w [mm·s^{-1}]	Δh [mm]
1400	500	10	0.53

To control the LMD-w system through Sinumeric 840D a NC code is required. The NC code for the translation is generated by a postprocessor integrated in Siemens NX and contains data about movement such as the path and traverse speed, necessary process data such as when to turn the wire feed and laser on, and other peripheries like argon feed. For the correct NC code generation, it is necessary to select the exact machine setup in Siemens NX CAM, including the substrate with the part to be manufactured. To generate the path for the control system, a sketch of the part's geometry is required. The parts were positioned to fit 4 depositions on one substrate, ensuring they did not interfere with each other, as illustrated in Figure 7-4.

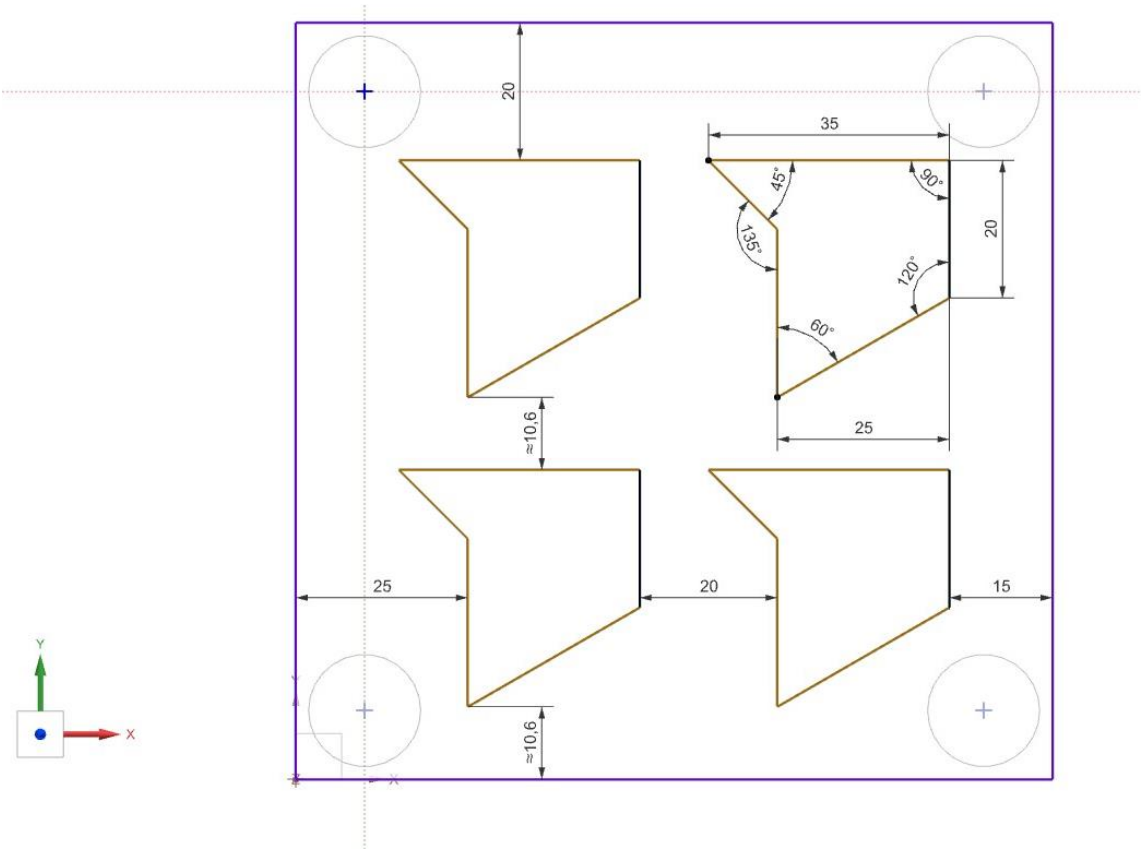

Figure 7-4: Position of the deposition on the substrate

The next step is to select a suitable operation and tool within Siemens NX to give information about kinematics and technology to the CAM. For this experiment, the “Planar Profile 2D” operation was selected, as it suits the simple kinematics of the designed part. The deposition is executed in plane XY with an increasing increment in the Z-axis direction which makes this operation the most appropriate option. The operation enables the setting of multiple parameters related to the kinematics, such as feed rate during the process, feed rate in a safe level from the substrate, the coordinate system, and engage and disengage strategies. The engage and disengage strategy, which affects the deposition has been set to “Plunge”. This setting defines that the tool approaches the start of the track along the Z-axis by a predetermined distance. The operation has been copied and translated in Z direction by 0.53 mm to create a 10-layer deposition.

After setting up the operation, the process can be verified for potential collisions or other issues during the setup by a simulation. The simulation can be set to leave a trace of the tool path to verify the expected path of the robot after it is completed. After the simulation, an NC code is generated by a postprocessor, containing the kinematics for the selected system, installed in Siemens NX. The simulation is shown in Figure 7-5.

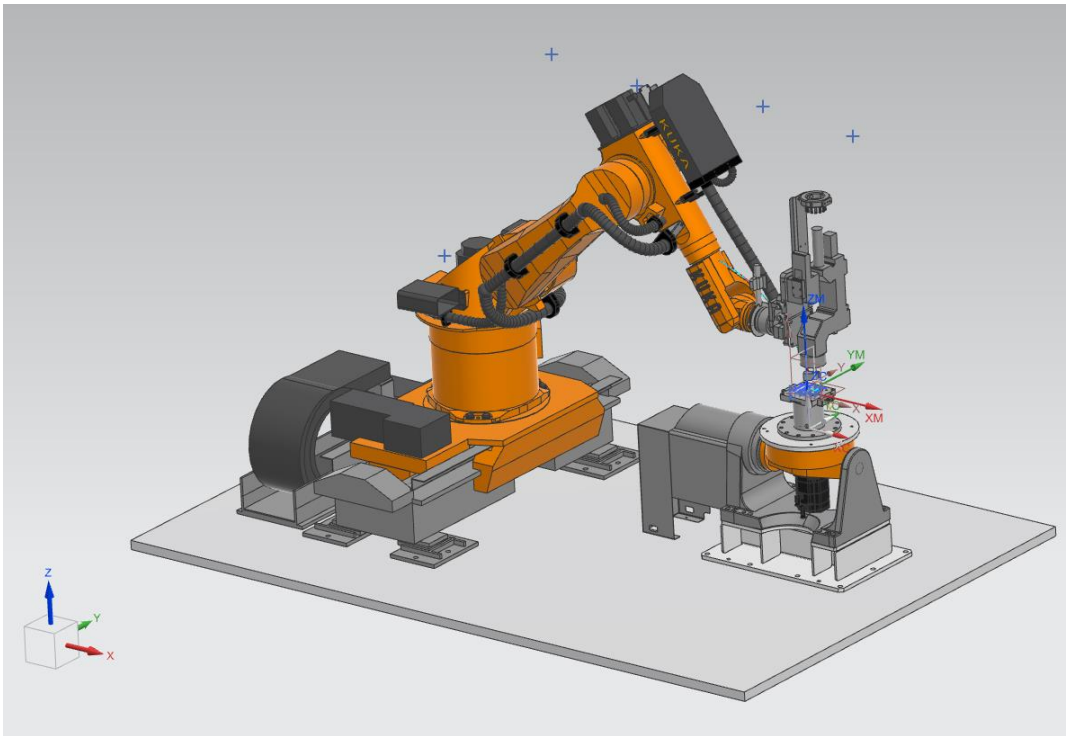

Figure 7-5: Simulation of the process in Siemens NX

8 Experimental part

8.1. Deposition without control

To validate the assumptions considered in this work, three parts each consisting of 10 layers, were deposited. During this process, no regulation was applied to control overfill in the corner sections of the part. Furthermore, position, speed, and wire speed data were collected and evaluated during the experiments. After the calibration of the laser's position relative to the wire tip and executing the NC program in dry run mode, the deposition commenced. Figure 8-1 shows the deposited parts, with a legend explaining the color coding and the corresponding heights of the deposition. The expected height of the part after 10 layers is 5.3 mm. The red sections indicate that the height of the part did not exceed this expected value, whereas blood red sections represent areas that have surpassed the height of 5.3 mm, thus being considered as overfill. It is visible that the highest overfill is in the section of the sharpest corners, specifically 60° and 45°, and the starting point of the deposition.

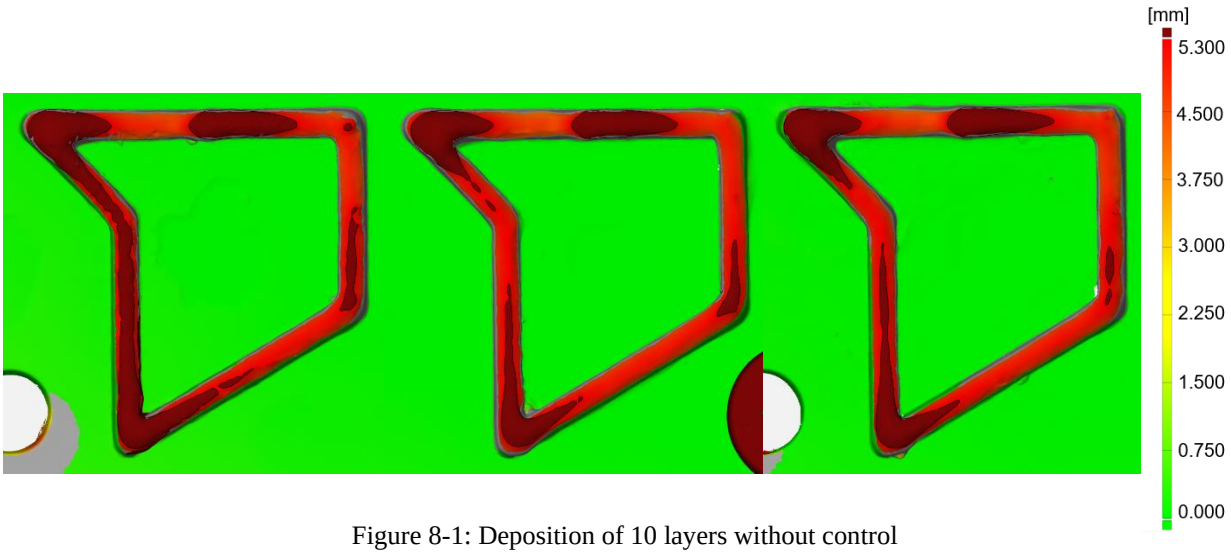

Figure 8-1: Deposition of 10 layers without control

The overfill at the starting point is caused by requirements for a stable process, where there is a delay between the beginning of the wire feed and the movement of the robot. This could be mitigated by a continuous deposition, where the height increment would be gained during the deposition of one layer, thus meaning the transition effect would occur only once. However, with continuous deposition, the substrate heats up due to the constant energy input from the laser. This increased temperature would lead to the previously described „mushroom effect“. The bead width would increase and the height would decrease, influencing the overall height

of deposition and negatively affecting the focus of research conducted in this work. For future applications, this problem could be addressed by melt pool temperature control through regulation of the laser power. By maintaining the constant temperature of the melt pool, the geometry of the beads would remain more consistent compared to a process without control.

The overfill in corner sections is expected to be caused by a combination of factors. A slowed traverse speed occurs in the vicinity of the corner section, where the speed vector changes direction and the beads overlap in depositions at sharp angle corners as shown in Figure 6-2. The overfill due to overlapping beads comes straight from the geometry of the tool path, the width of the bead, and the volume of wire fed. The overfill caused by the slowed speed is affected by the mechanics and control of the system. It will be unique for hardware setups and control systems, therefore, to understand the process within this system, position data were extracted and evaluated using the trace function. The control system gathered positional information at intervals of 4 milliseconds in the X, Y, and Z coordinates of the G54 coordinate system. The position data were filtered to show only the deposition process as depicted in Figure 8-2.

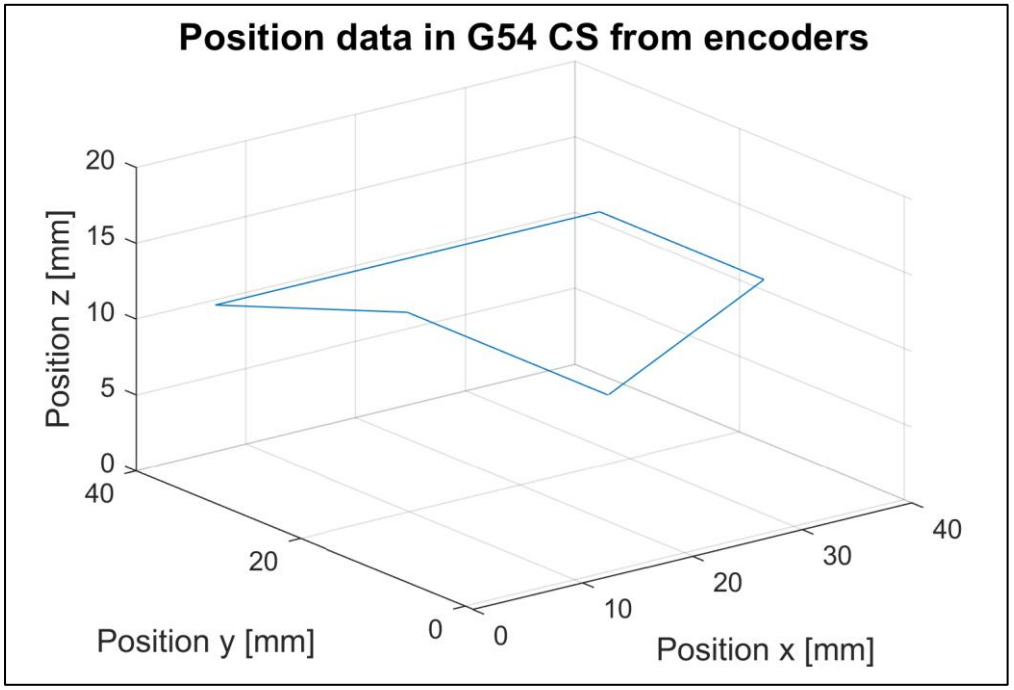

Figure 8-2: Processed position data from the control system

With the position data and the sampling rate known, the velocity could be calculated by a derivative of the position data with respect to time. The velocity for each axis has been calculated using the "diff(p)" function in Matlab 2023b which is represented by Formula 7.1

$$\vec{v}_c = \frac{d\vec{p}_c}{d\vec{t}} = \frac{diff(\vec{p}_c)}{diff(\vec{t})} = \frac{[p_c(2) - p_c(1); \dots p_c(n) - p_c(n-1)]}{[t(2) - t(1); \dots t(n) - t(n-1)]} \quad (7.1)$$

where c = X, Y depending on the position vector for each axis, $\vec{v}_i$ [mm·s^{-1}] is the corresponding velocity vector, $\vec{p}_i$ [mm] is the corresponding position vector and $\vec{t}$ [s] is the time vector. The velocity in the direction of the Z axis is considered zero while depositing a single layer and not changing the Z level continuously through the deposition which is the case in this experiment. The speed vectors for each direction themselves do not give much information about the speed development in the XY plane in total. To calculate the traverse speed in the XY plane during the deposition the Pythagorean theorem was used,

$$v_t(i) = \sqrt{v_x^2(i) + v_y^2(i)} \quad (7.2)$$

where i = 1,2…n, v_t [mm·s^{-1}] is the traverse speed, v_x [mm·s^{-1}] is the velocity in the X direction and v_y [mm·s^{-1}] is the velocity in the Y direction. The traverse speed and the velocities in the X and Y directions in time of the deposition's duration are shown in Figure 8-3.

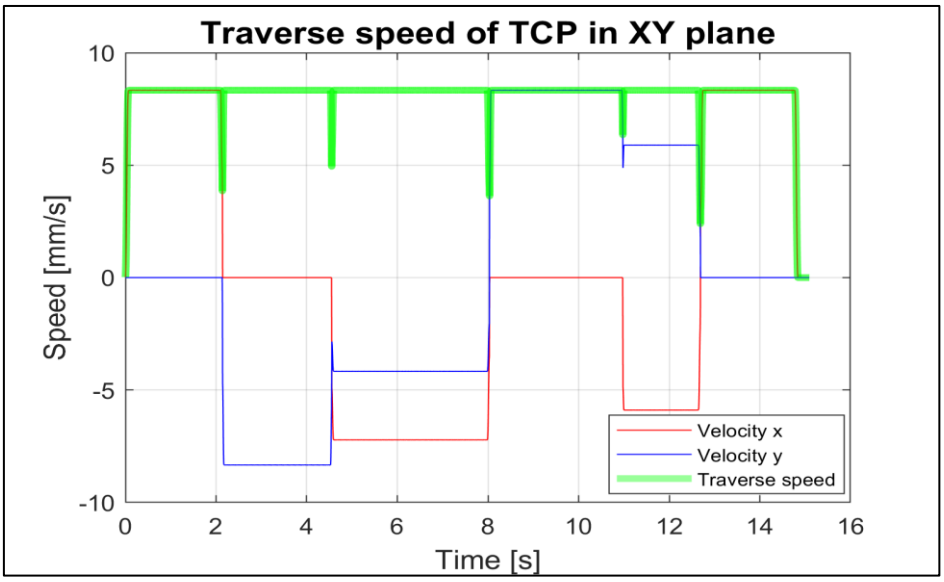

Figure 8-3: Traverse speed of the TCP in time of the depositions duration

It is visible that the traverse speed has dips in areas where the velocities change directions from negative to positive and vice versa. In areas without a change in velocity direction, the traverse speed remains at the programmed value of v_t = 8.333 mm·s^{-1}. The traverse speed in time does not give a clear visualization of where the dips occur. For this reason, the traverse speed was projected in Figure 8-4 dependent on position, rather than time.

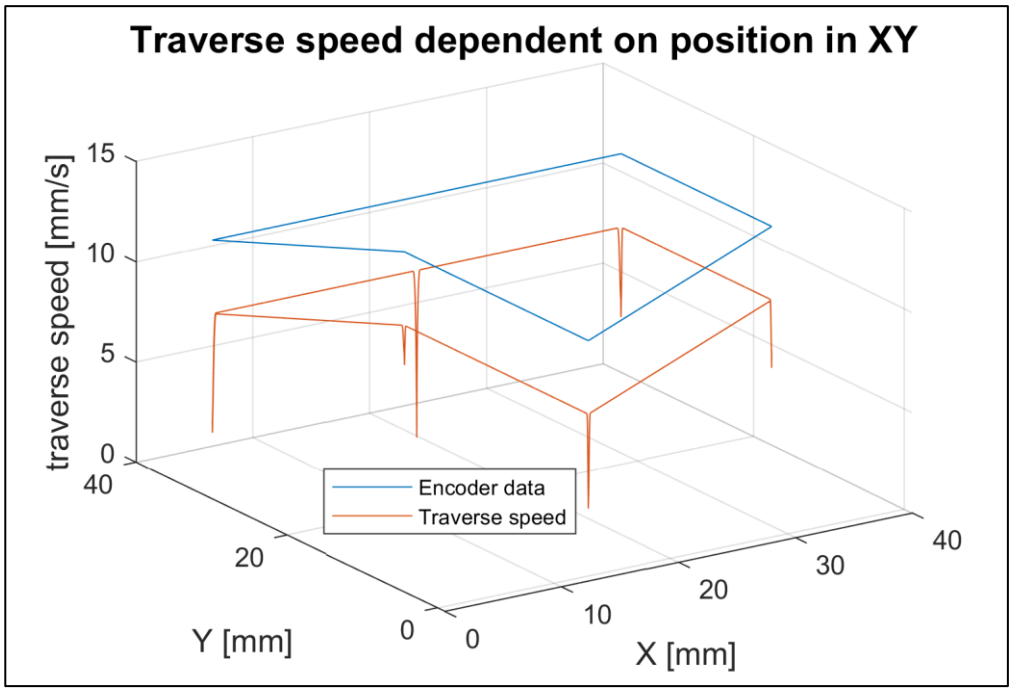

Figure 8-4: Traverse speed dependent on position

This figure shows that the speed decrease occurs in the vicinity of the corner sections, thus giving more time to feed the wire into the area, resulting in overfill. It can be seen that the sharper the corner is, the lower the traverse speed dips. A closer view of the effect of the sharpness of the corner on the traverse speed progress is visible in Figure 8-5, where the true speed is compared to the demanded speed. The sharper the corner, the lower the minimum and average speed are, with the values for each corner presented in Table 6.

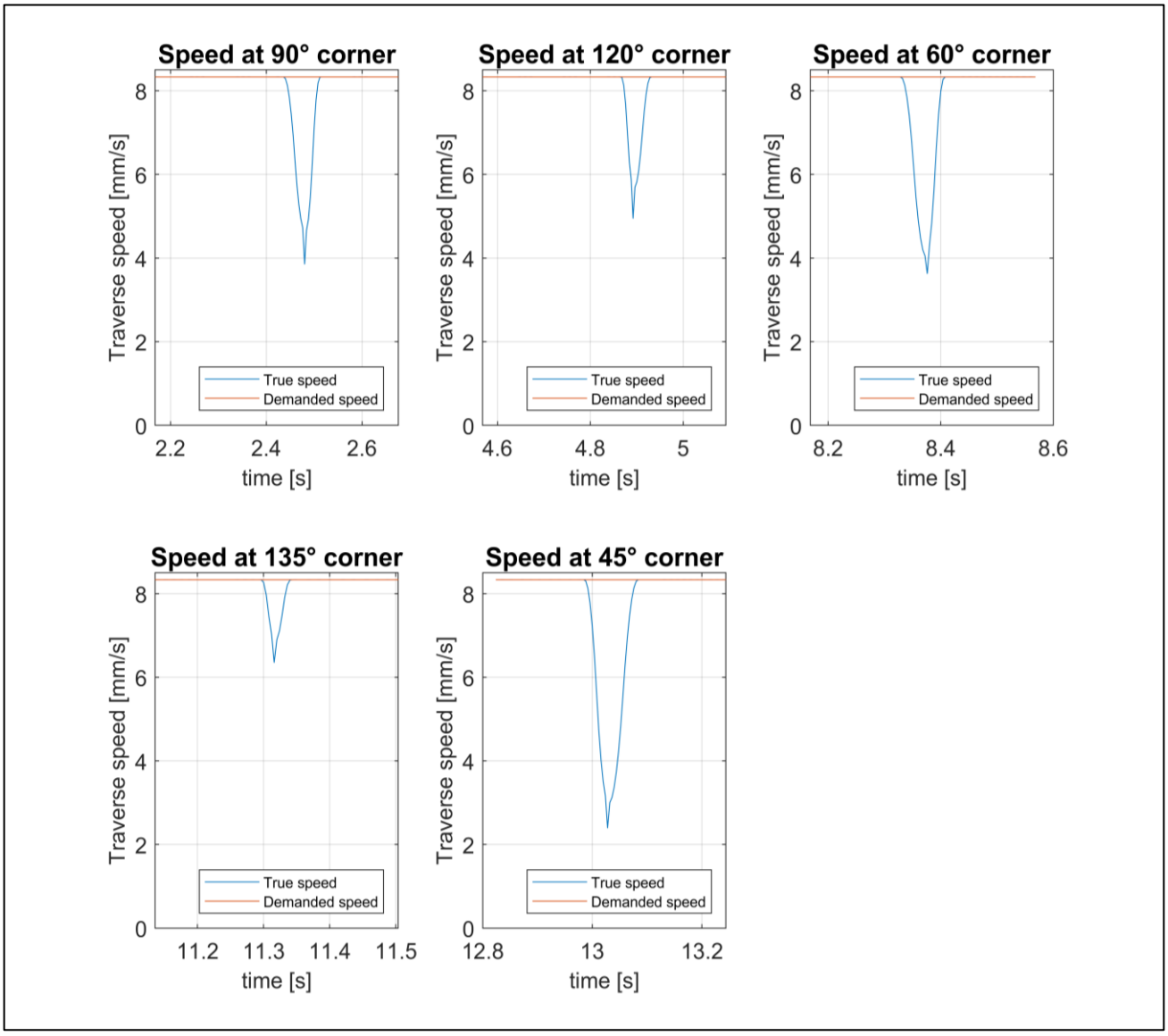

Figure 8-5: Progress of traverse speed in movement through differently sharp angles

Table 6: Minimum and average speed values for different corner angles

Corner	45°	60°	90°	120°	135°	Demanded
Minimum speed [mm/s]	2.4	3.63	3.86	4.95	6.35	8.33
Average speed [mm/s]	5.8	6.34	6.62	7.1	7.67	8.33

The data from the control system have shown that the sharpness of the corner predictably influences the true speed of the Tool Center Point (TCP). The sharper the corner is, the greater the change of speed vector and, the greater the decrease in speed. However, this data originated from encoders, giving only the theoretical position of the TCP. The real position of the TCP is subjected to errors such as joint flexibility when compared to the encoder data [103] and the interpolator rounds the TCP path in the corner sections. [104] To capture the true position of the TCP and verify the precision of the encoder data, an absolute laser tracker was used. The laser tracker was placed inside the laser cell and the reflector was placed on the deposition head as shown in Figure 8-6.

Figure 8-6: Laser tracker setup

The program was executed in a dry-run mode, set to automatic, to ensure the same movement conditions of the robot as in the deposition process. The position data from the laser tracker can be configured to either the cartesian coordinate system of the tracker or its angular coordinate system. For simplicity of comparison with the encoder data, the output was set to the cartesian coordinate system. After retrieving the position data from the laser tracker, they had to be processed to show only the position data from the deposition. Both the compared position data were in different coordinate systems, the data from the control system in the G54 coordinate system of the robotic cell and the laser tracker data in the coordinate system of the laser tracker as illustrated in Figure 8-7.

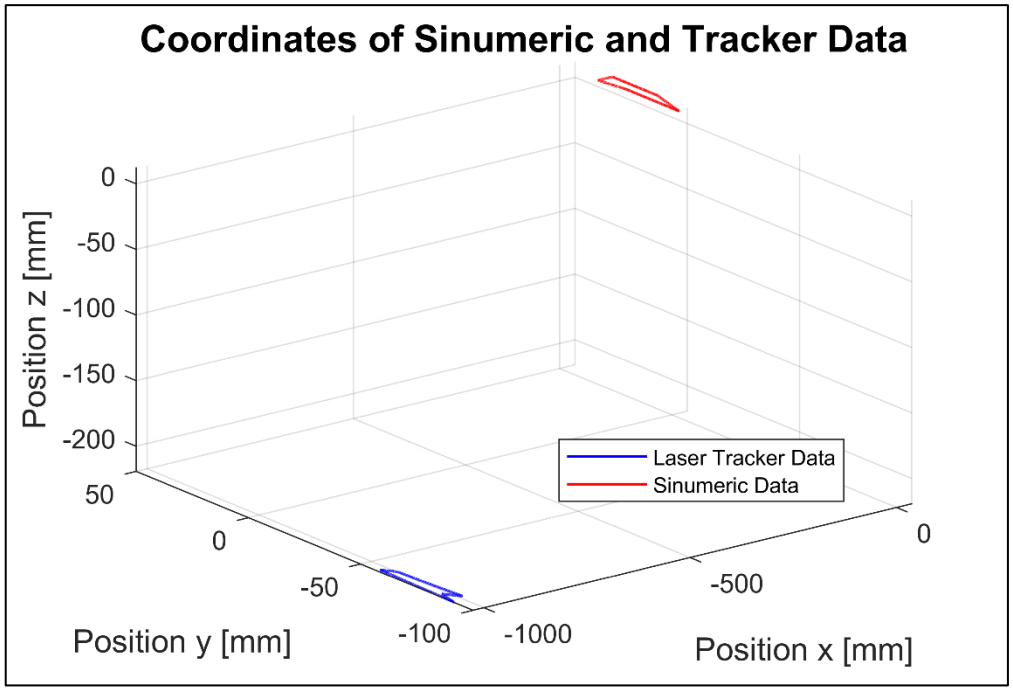

Figure 8-7: Position data from Sinumeric and laser tracker in their original coordinate systems

For direct comparison, the data needs to be transformed on one another using transformation matrices. The laser tracker had a sampling time of 1 ms, whereas Sinumeric gave the position data every 4 ms. To be able to transform the laser tracker data into the G54 coordinate system, it is necessary to linearly interpolate the Sinumeric data to match the size of position vectors of the laser tracker data. At first, the angle between the longest bases of the deposited geometry in the XY plane was calculated through vectors between points near the corners bounding the base of the geometry and the transformation matrix rotating around the Z-axis $R_{\varphi z}$ was applied to the laser tracker data

$$R_{\varphi z} = \begin{bmatrix} \cos(\varphi_z) & -\sin(\varphi_z) & 0 & 0 \\ \sin(\varphi_z) & \cos(\varphi_z) & 0 & 0 \\ 0 & 0 & 1 & 0 \\ 0 & 0 & 0 & 1 \end{bmatrix}$$

where φ_z [rad] is the angle between the vectors in the XY plane. The angles in the XZ and YZ were neglectable and difficult to determine due to the noise of the laser tracker data. After aligning the data angularly, the laser tracker data were transformed onto the Sinumeric data using the translation transformation matrix in X, Y, and Z directions T.

$$T = \begin{bmatrix} 1 & 0 & 0 & T_x \\ 0 & 1 & 0 & T_y \\ 0 & 0 & 1 & T_z \\ 0 & 0 & 0 & 1 \end{bmatrix}$$

Where T_x [mm] is the distance in the X-axis direction, T_y [mm] is the distance in the Y-axis direction and T_z [mm] is the distance in the Z-axis direction. After the transformation, the data could be compared to one another including the speed. The aligned data can be seen in Figure 8-8.

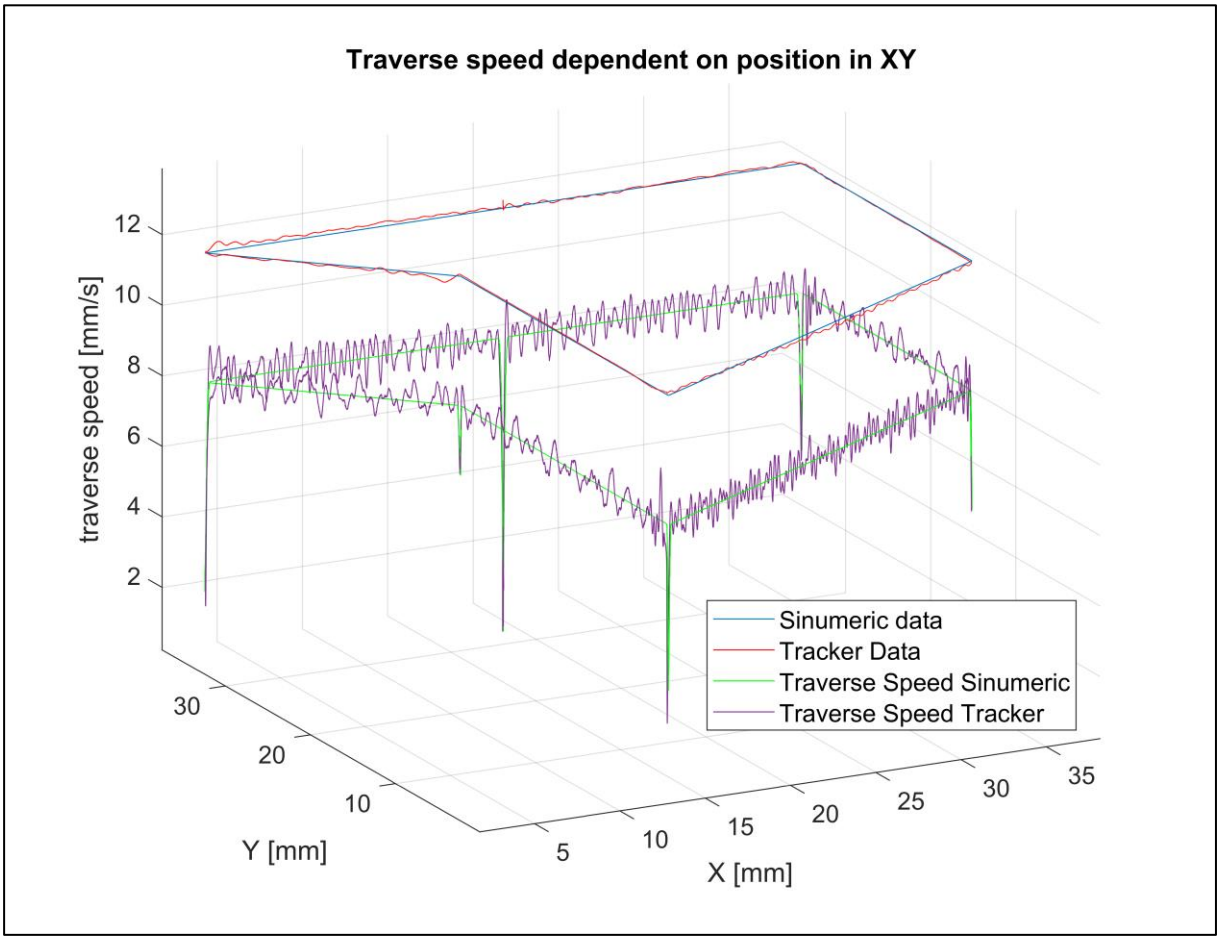

Figure 8-8: Aligned position and speed data from Sinumeric and laser tracker in the G54 coordinate system

The noise in the traverse speed calculated from the laser tracker data is caused by the high resolution, and noise of the position data from the laser tracker and also by the fact that the speed of a real mechanical system is not constant but rather oscillates around the set value. For comparison the mean value of the traverse speed from the laser tracker data on straight sections

was $v_{t\_tracker} = 8.264\ mm/s$ compared to the theoretical value of $v_t = 8.333\ mm/s$. A more detailed view of the speed progress in the corner sections is illustrated in Figure 8-9.

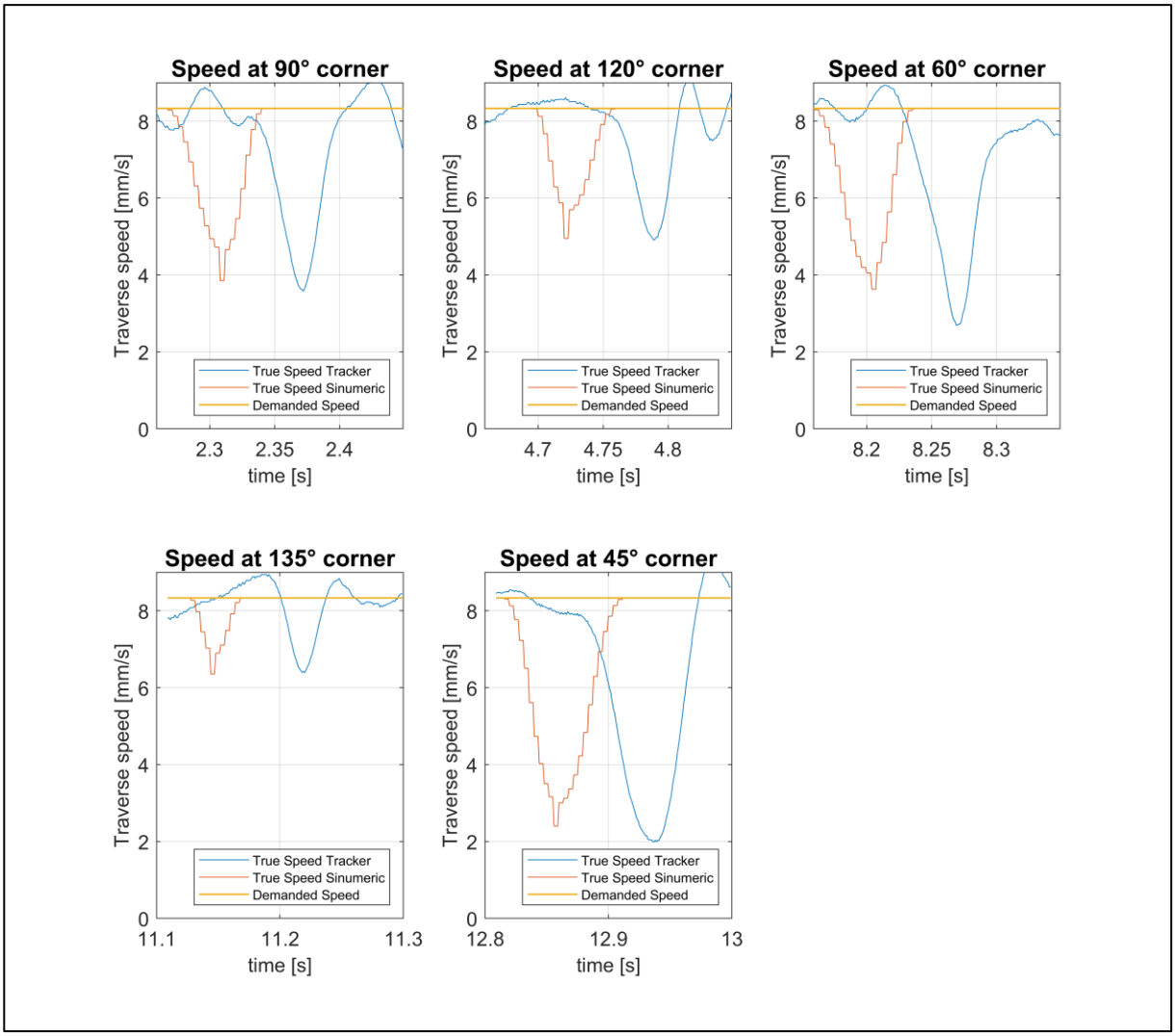

Figure 8-9: Comparison of the progress of traverse speed in corner sections for Sinumeric and laser tracker data

The position of the speed dips does not align perfectly with one another, which can be caused by the transformation of the data on the noised data from the laser tracker. More importantly, the progression of the traverse speeds is similar in both the data from Sinumeric and the laser tracker, meaning that the Sinumeric is reliable in providing speed information. The difference between the pair of data can be seen after a close-up of the corner sections of the position data. The Sinumeric data show the TCP path with a sharp corner that has no radius, in reality, the interpolator of the control system creates radii around the corner sections to smoothen up the

movement of the system as is shown in Figure 8-10. These observations are consistent with findings in the literature [104].

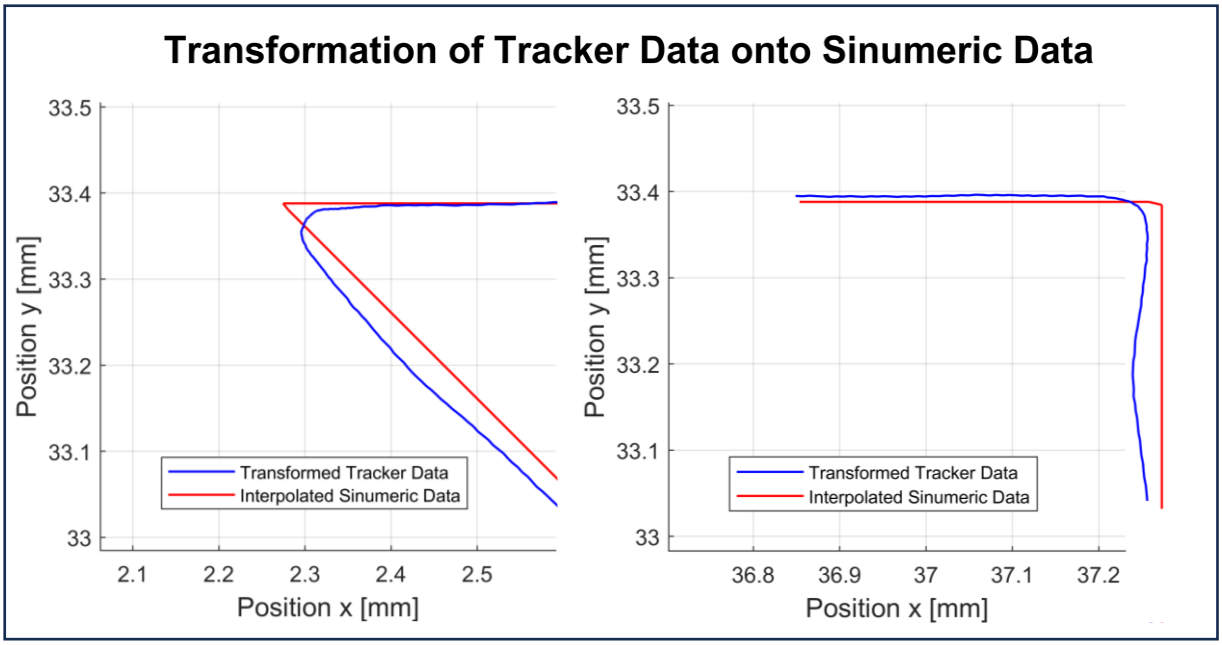

Figure 8-10: TCP path from Sinumeric and laser tracker

8.2. Deposition with closed-loop control function

One of the goals of this study is to activate and verify closed-loop control functions already implemented by the contractor who assembled this robotic cell with all the technologies. The function controls the wire speed depending on the actual speed of the robot. It is supposed to mitigate the overfill caused by the deviation of the actual robot speed compared to the demanded robot speed. The exact configuration of the function is unknown, as it is programmed within the PLC project that is inaccessible to the operator of the system. Without access to the PLC project, the operator cannot modify the function but can only adjust a user parameter “k” [-] within the range of [0-0.99]. The parameter changes the sensitivity of the function, determining how steeply the wire feed rate will be reduced relatively to the ratio of true robot speed to the programmed robot speed. To create a control strategy, the function and the influence of the *k* parameter were verified experimentally. The initial experiments were conducted within the whole range of the user parameter and the exact values are visible in Table 7. Values were chosen in increments of 0.2, starting at k = 0.001, since a value of 0 disables the function. The upper limit tested was k = 0.99. To activate the function a license had to be enabled and a

command for the value of the sensitivity parameter needed to be included in the NC code of the program.

Table 7: Designated numbers of test parts with their associated values of parameter k

Nr.	I.	II.	III.	IV.	V.	VI.	VII.
k	0.001	0.2	0.4	0.6	0.8	0.99	-

The experiment proceeded in the same way as with the deposition without control. 10 layers were deposited for each value of the sensitivity parameter and afterwards, the deposition would be scanned by the 3D scanner. The scanned parts are visible in Figure 8-11 with the same color legend as previously.

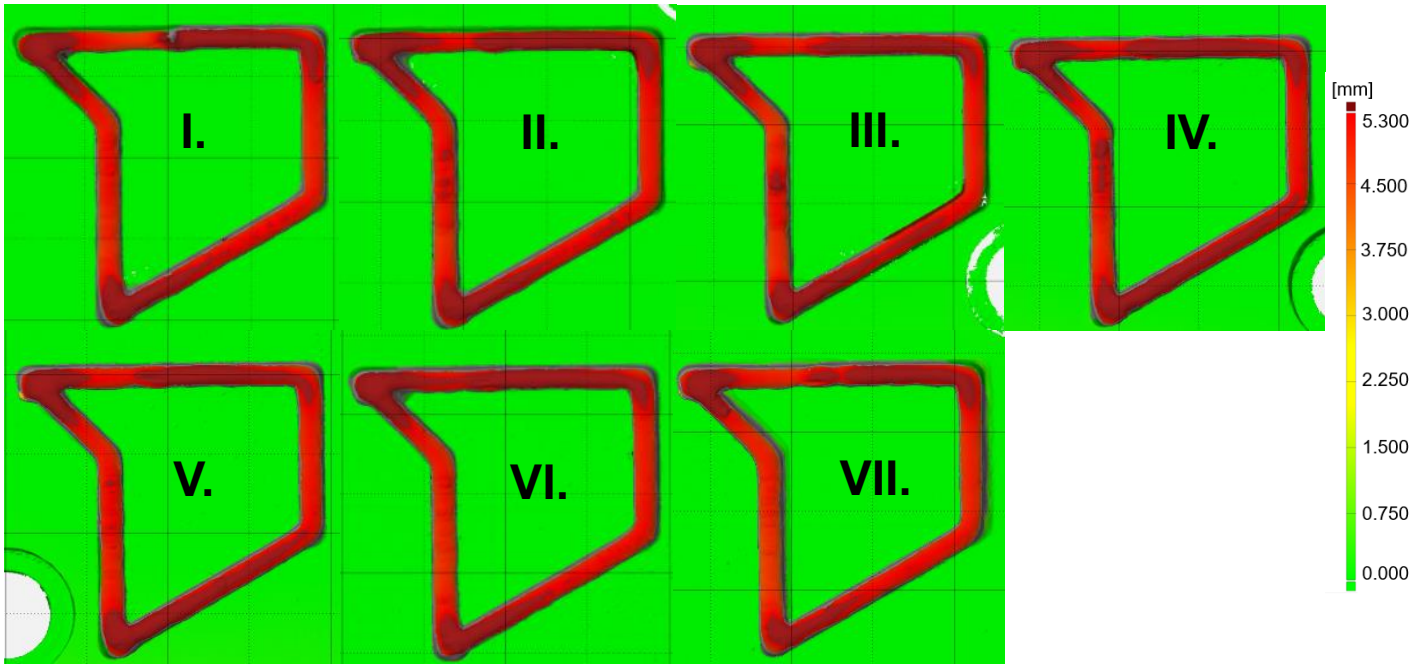

Figure 8-11: Overfill evaluation of test parts with different values of the parameter k

It is visible that regardless of the value of the parameter *k*, the function fails to solve the overfill in sharp corners sections. To confirm that the function truly does control the wire feed rate, data from the wire feeding unit were extracted using Abicor Binzel monitoring software. The software enables monitoring of various variables, such as motor current on the encoders, length of wire delivered, the bit signal value of feeding the wire, and more. Most importantly for this

work, it monitors the speed of the encoder feeding the wire. The interface of the software can be seen in Figure 8-12.

Figure 8-12: Interface of the Abicor Binzel monitoring software

This screen is for one layer deposition with the parameter k = 0.001 and there are 2 visible dips in the wire speed. However, since the robot's speed decreases at each of the 5 corner sections, the signal does not display the information as expected. To gain a better understanding of the process, the wire speed data were imported into Matlab R2023b, offering enhanced data handling and viewing abilities than the Abicor Binzel software. Figure 8-13 shows 2 logs for 2 different layers deposited with the k parameter set to 0.001. The blue line shows the actual encoder speed measured by the sensors and the red line shows the demanded speed sent from the PLC. For unknown reasons, the data from the wire feeder have an offset from the programmed value stated in the NC program.

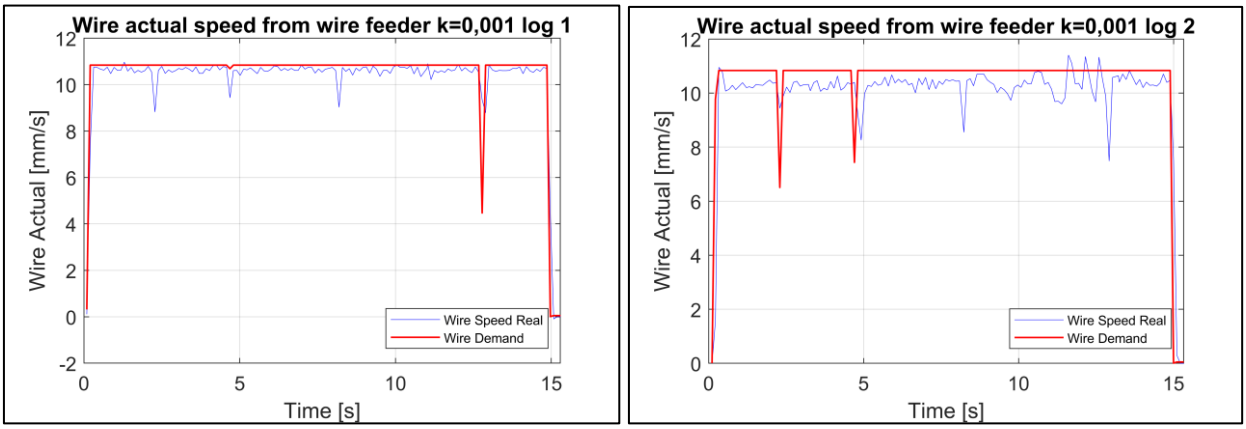

Figure 8-13: Wire speed progress captured for 2 different layer deposition for k = 0.001

Both of the logs have 4 dips of the actual speed of the encoder, representing the 4 angles of 90°, 120°, 60° and 45°. The magnitudes of the actual speed dips, as well as the number of dips in the demanded speed, are inconsistent. This inconsistency is likely due to the wire feeder's sampling time, which cannot be set below 120 ms. As discovered from Figure 8-5 and Figure 8-9 the slowed movement in the corner sections lasts approximately 100 ms hich implies that while the system can capture data on wire speed changes due to robot speed, it is not guaranteed to do so. This also explains the lack of wire speed dip in the 135° corner section, as the duration of reduced traverse speed is the shortest at this angle. The demanded value and the true value of the encoder speed is also expected to have a short delay, which can be seen at the start and end of the process where the blue line tracks the red line. This clarifies the captured data containing actual speed dips without a corresponding demanded speed dip, simply because it wasn't captured at the precise moment within the sampling frequency. This element of randomness can be reduced by increasing and overlapping the number of measurement logs as it is similar to uncertainty of A type. In Figure 8-14 are 10 logs captured for each layer of the deposition with k = 0.001.

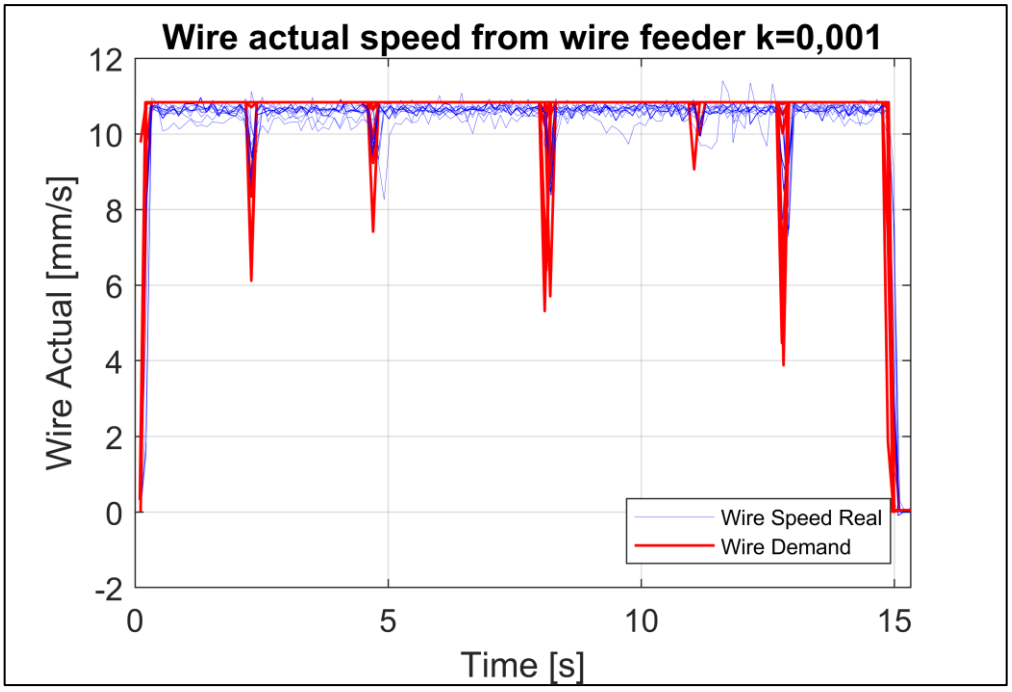

Figure 8-14: wire speed progress for all 10 layers for k = 0.001

With more sets of visualized data, some of the logs managed to capture the missing information from the first 2 logs. Figure 8-14 demonstrates, that for this parameter, the function did reduce the wire speed in every corner. To see the difference between the values of the k parameter on the wire speed, the encoder speed for k = 0.4 and k = 0.99 was also analyzed. Figure 8-15 displays the signal for both values of parameters.

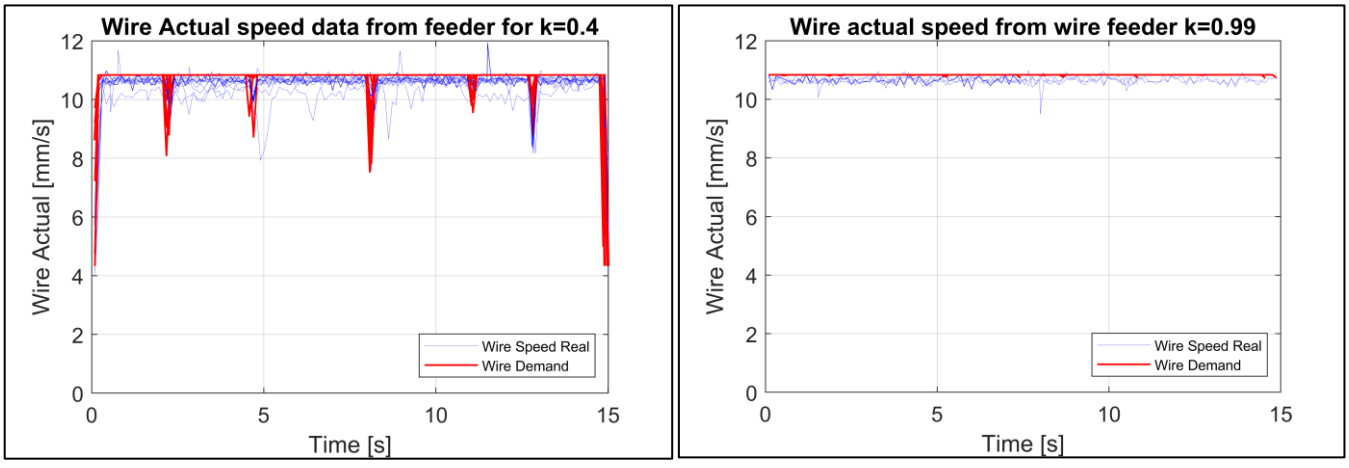

Figure 8-15: Wire speed captured for k = 0.4 and k = 0.99

When comparing the three values of the sensitivity parameter, and their influence on the function's ability to reduce wire speed based on traverse speed, a pattern emerges. The sensitivity of the function is inversely proportional to the value of the k parameter; the lower

the k value, the higher the function's sensitivity. At a value of k = 0.001, the PLC sent a signal with the sharpest dips in the demanded encoder speed into the wire feeder, while at the value of k = 0.99, there were no noticeable speed dips in the demanded speed signal nor the actual speed signal.

9 Results and Discussion

The experimental phase confirmed the assumptions that during the deposition of geometries with sharp corners a material overfill occurs in the vicinity of these corner sections. These findings align with the literature as the overfill is caused by a combination of overlapping beads and the slowed movement of the deposition head due to the change of direction. With a sharper angle, the area of overlapping beads increases and the traverse speed decreases, meaning that the sharper the angle is the greater the overfill is. Since overfill critically affects process stability, implementing a control mechanism to mitigate this issue is necessary. The contractor installed a control function in the PLC project to regulate wire speed based on the ratio of the actual robot speed to the programmed robot speed. The operator defines a value of the parameter "*k*", that modifies the wire speed reduction rate. From the experiments, it is known that the function is more sensitive with the lower values of the parameter. However, the deposited part did not show any major improvement in controlling the overfill in the corners regardless of the set parameter value. The control function only considers the traverse speed reduction but does not reflect the overfill caused by the overlapping beads. Since the PLC project is accessible only to the contractor, the function cannot be modified by others. Consequently, it is inadequate for controlling overfill in the corner sections. A strategy with a different approach is presented in the next section.

9.1. Proposal of a control strategy

Several closed-loop control strategies for LMD-w, found in the literature, have proposed the use of various sensors for height measurement and calculations including CCD cameras, laser line scanners, OCT sensor, and a structured light scanner. The controlled variable was exclusively the wire speed, as compared to the LMD-p process wire has minimal response delay to changes. Since this work preconditioned the possibility of using and debugging the implemented closed-loop control function described in the previous sections, the available sensors for height measurement are limited to the structured light scanner previously used for parts measurement. This 3D scanner will serve as the sensor to determine the overfill in corner sections after the deposition of a certain number of layers. The scanner is not suitable to be mounted on the robotic manipulator or the deposition head due to its size and weight and requires a special stator. For safety reasons, the 3D scanner is kept outside the robotic cell during the deposition and is then manually transported inside the cell to scan the deposited

geometry. As previously mentioned, with this stator configuration, scanning must be manually executed using a computer that operates the scanner. The measured data are to be evaluated and based on the results the wire speed is to be regulated at the desired position. Since there is no direct connection between the scanner's computer and the control system, and establishing such functioning communication is above and beyond the scope of this thesis, the validation of the strategy and its functionality will be verified through an offline closed-loop control procedure. This means that an operator is necessary to conduct the measurements, evaluate the data and change the variables in the NC code. The control strategy diagram is shown in Figure 9-1.

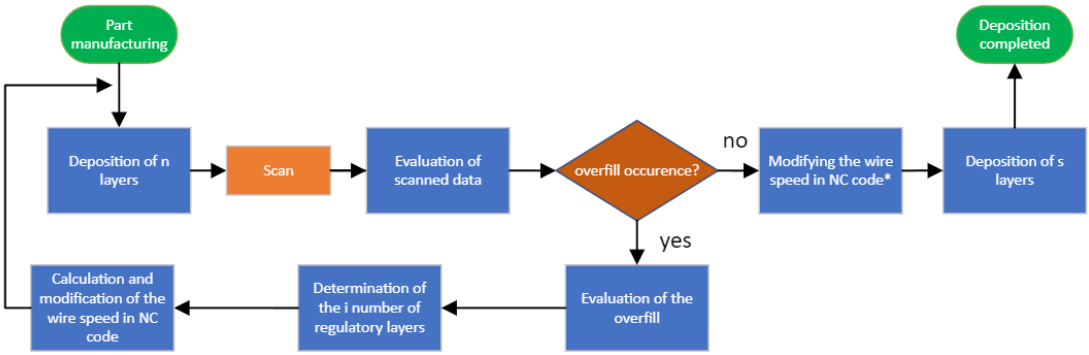

Figure 9-1: Control strategy diagram

When manufacturing a part consisting of a predefined number of layers, the deposition will be halted after depositing *n* number of layers. Afterwards, the part will be measured by the structured light scanner and the data are to be evaluated to determine if there is an overfill or not. In case of a non-existing overfill, the process parameters do not need to be modified and the deposition can be completed with the current NC program by depositing *s* number of layers. This could be the case for depositions without sharp corners such as pipe-like geometries. However, if there is a detected overfill, its volume and dimensions are evaluated, and a number of regulatory layers *i* is then determined. The new wire speed is calculated based on the results from the following formulas,

$$V = \frac{\pi \cdot d_w^2}{4} \cdot \left(\frac{L}{v_t} + t_d\right) \cdot v_w \tag{9.1}$$

$$\Delta V = \frac{\pi \cdot d_w^2}{4} \cdot \left(\frac{L}{v_t} + t_d\right) \cdot v_w - \frac{\pi \cdot d_w^2}{4} \cdot \left(\frac{L}{v_t} + t_d\right) \cdot v_{wr} \tag{9.2}$$

where V [mm^3] is the volume deposited with a wire of diameter d_w [mm], wire speed v_w over the length L [mm] with the traverse speed v_t, and also the time the system was delayed in a corner section due to the reduced speed by time t_d [s]. ΔV [mm^3] is the desired volume difference and v_{wr} [mm/s] is the regulatory wire speed to achieve the volume difference. The volume will be measured through the Autodesk Fusion 360 software based on the cut-out mesh from the 3D scanned data. The scanned data will be processed in the scanner inspection software ATOS Professional. The NC code will be modified afterward so that the wire speed will be regulated at a distance before the corner section to the calculated regulatory wire speed as is depicted and returned to the programmed wire speed at a defined distance after the corner section as is depicted in Figure 9-2.

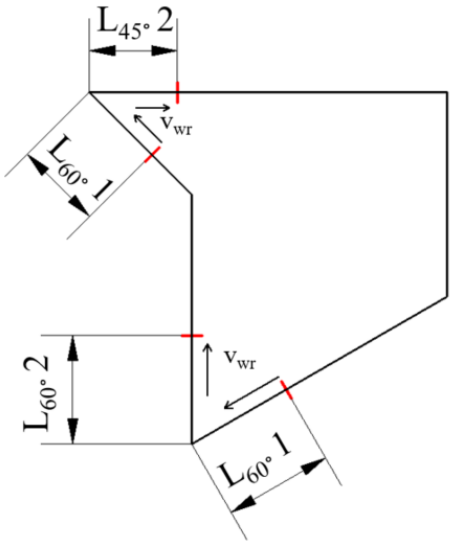

Figure 9-2: Graphical representation of the areas with modified wire speed

9.2. Verification of the control strategy

The experimental verification of the control strategy was conducted on the 10-layered depositions shown in Figure 8-1. The most right deposition was used as a test piece to detect potential complications. The parts were scanned after the deposition while the substrate was clamped to the table to ensure no displacement before the subsequent deposition of the regulatory layers. The scanning setup can be seen in Figure 9-4.

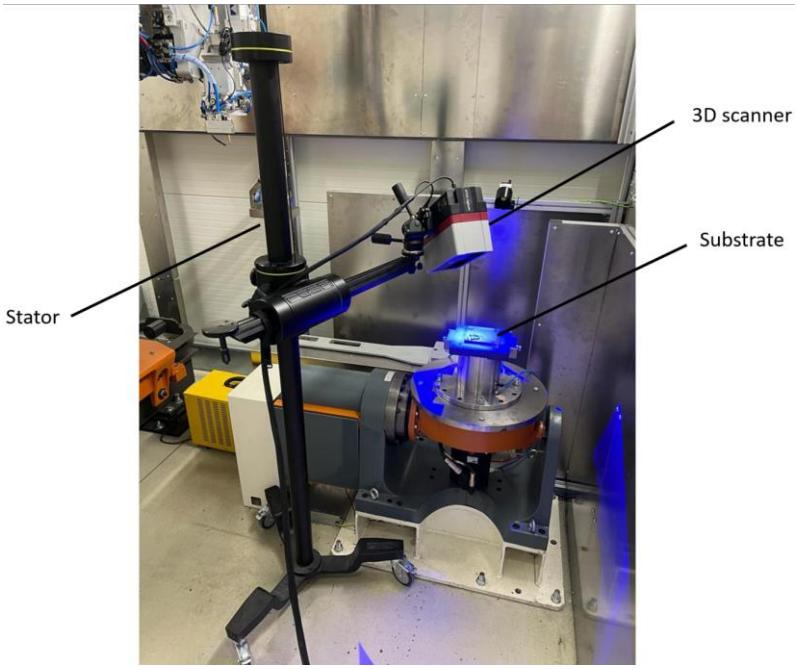

Figure 9-4: Structured light scanner setup

The scanner was positioned at different angles to capture the deposition and to increase the quality of the subsequently generated mesh. Once the mesh is generated, it is aligned with the CAD model of the substrate plate using the best-fit alignment method, as depicted in Figure 9-3. The alignment with the CAD model of the substrate plate ensures that the mesh is situated in the global coordinate system of the inspection software and the Z-axis of the global coordinate systems in the direction of the deposition.

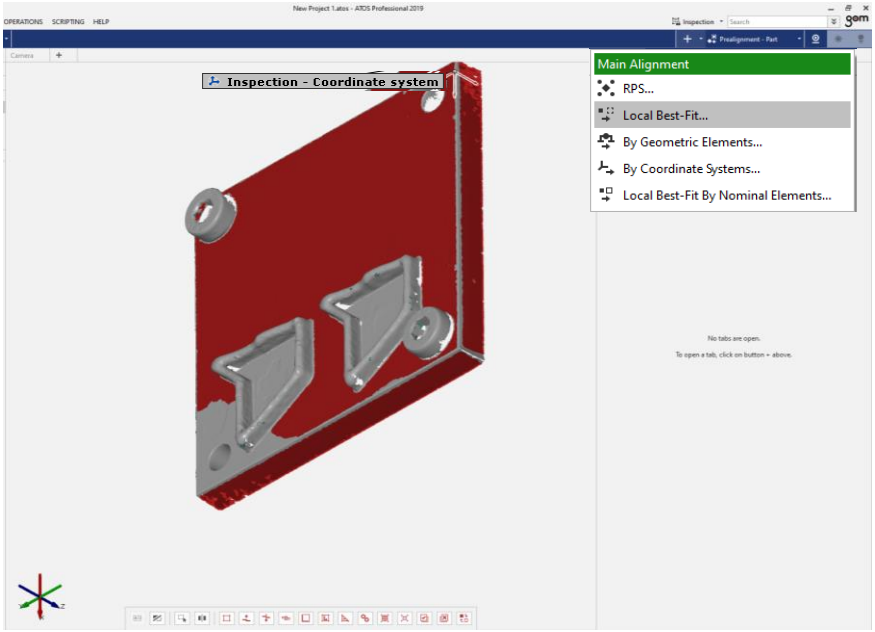

Figure 9-3: Mesh alignment onto CAD data by the “Local Best-Fit” method

Following the alignment, the overfill is detected by creating a deviation map of the mesh from the CAD model of the plate. This map uses a colored legend to highlight areas where the part exceeds the expected height of 5.3 mm. To measure the overfill lengths relative to the corner points, points in the corner sections and lines were constructed on the mesh. These markers represent the deposition path and assist with the length's determination. The starting and ending points were not always clear, as small deviations above the 5.3 mm height also occurred that had not been caused by the overfill in the corner sections as illustrated in Figure 9-5. In such cases, the length was considered to be symmetrical to the corner point as either the start or the end of the overfill in the corner sections was always identifiable.

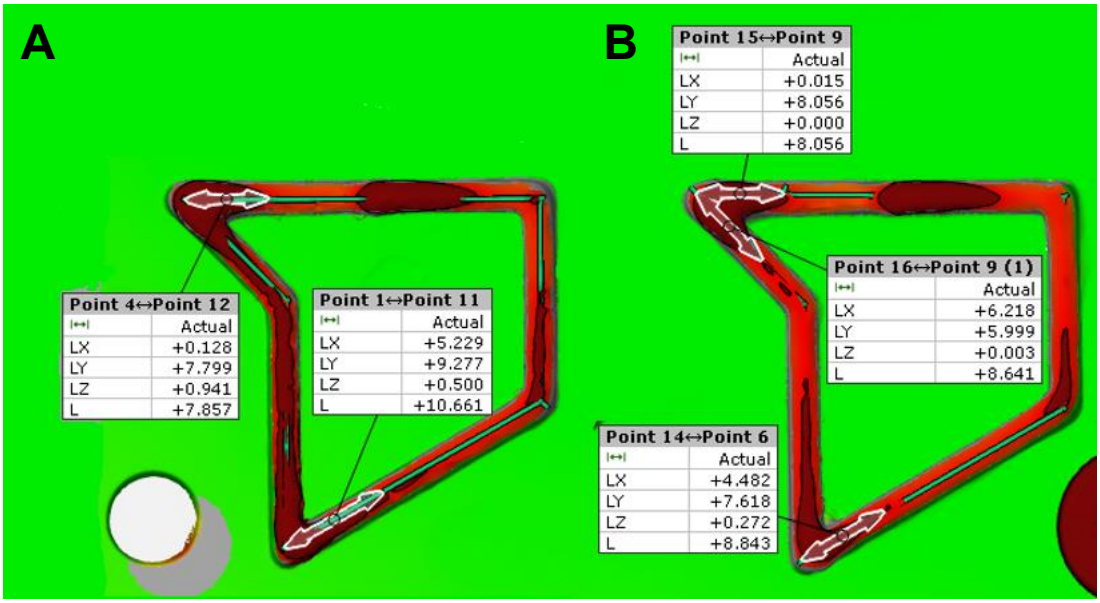

Figure 9-5: Methodology for evaluating the lengths of overfills in corners

After acquiring the distances the mesh was cut out below the height of 5.3 mm leaving only the corner overfills and other minor deviations from the height. To separate the corner overfills from the remaining mesh, all disconnected parts were removed. When the overfills were not separate, spheres were created with their centers at the corner points and diameters equal to the measured lengths for each corner. These spheres helped determine the overfill boundaries, and any mesh outside these spheres was also deleted. This process separates the overfills from the

rest of the mesh and the volume of the overfills can be subsequently measured. The operation of extracting the overfills from the 3D scan is illustrated in Figure 9-6.

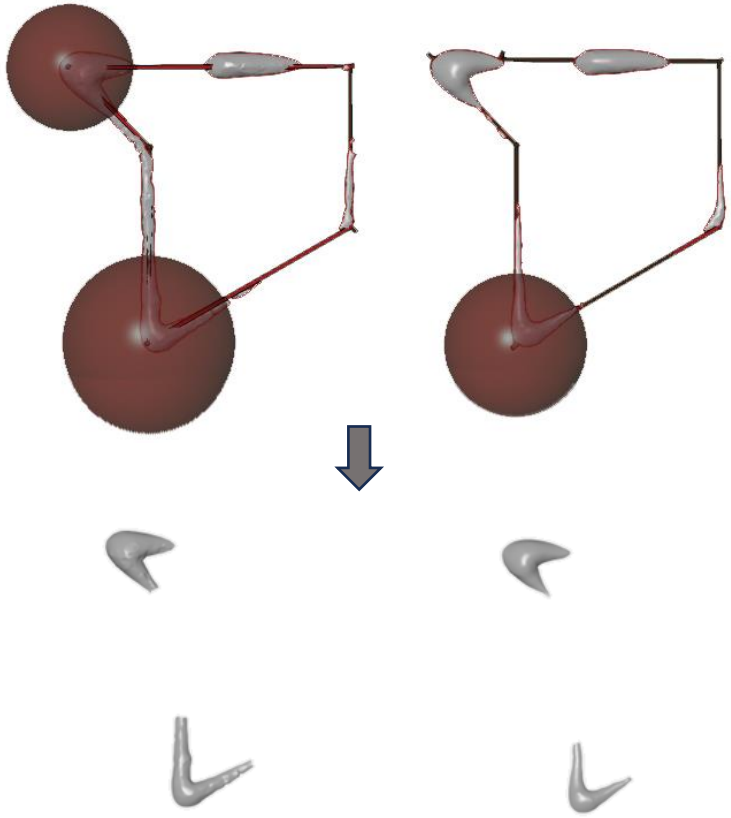

Figure 9-6: Methodology of overfill separation from the remaining mesh after the cut-out

The hollow meshes were imported into the Autodesk Fusion 360 software where they were stitched and repaired, and their volume was measured. The volumes and lengths of the overfills are shown in Table 8. As expected, the 45° corners had a higher volume of overfill than the 60° corners.

Table 8: Values of volume and distances of the overfills

Deposition	Overfill [mm^3]		Length of overfill [mm]			
	45°	60°	$L_{60°}1$	$L_{60°}2$	$L_{45°}1$	$L_{45°}2$
A	28.816	14.559	10.66	10.66	7.86	7.86
B	22.64	6.216	8.84	8.84	8.64	8.06

The remaining unknown variables are the number of regulatory layers i and the regulatory wire speed v_{wr}. The number of regulatory layers was set to i = 10 and the regulatory wire speed was

calculated from Formula 9.2. To achieve a deposition of the desired size after adding another 10 layers, the regulatory wire speed must be calculated based on twice the measured overfill volume. This is because the overfill already present on the part means that calculating the regulatory wire speed from the current volume would only prevent additional overfill, not reduce the existing amount. For the 10 regulatory layers, the amount of overfill volume must be missing from the deposition to balance the structural geometry of the part. All the variables and the resulting regulatory wire speeds are visible in Table 9.

Table 9: Variables for the calculation of the regulatory wire speeds and corresponding results

Dep.	Volume [mm^3]		*i*	Volume p. layer [mm^3]		d_w [mm]	L [mm]		t_d [s]		v_t [mm/s]	v_w [mm/s]	**v_{wr} [mm/s]**	
	45°	60°		45°	60°		45°	60°	45°	60°			**45°**	**60°**
A	57.6	29.1	10	5.76	2.91	1.2	15.7	21.3	0.1	0.08	8.333	10	**6.97**	**8.83**
B	45.3	12		4.53	1.24		16.7	17.7					**7.68**	**9.42**

The regulatory wire speed and the measured lengths of the overfill are then used to modify the NC code as described above. The X and Y coordinates of the starting and ending points are calculated from the coordinates of the corner points and the demanded distances. During the testing of the modified NC code, it was discovered that the function controlling wire speed within the NC program causes an interruption in the robot's movement. This results in a brief delay during which the wire speed is adjusted, yet the deposition head remains stationary. This resulted in undesired material accumulation at the points where the wire speed was accelerated from the regulatory wire speed back to the programmed wire speed. This issue significantly influenced the results of the control strategy, as can be seen in Figure 9-8.

Figure 9-8: Material accumulation due to wire speed acceleration and movement interruption

The points where the wire speeds were modified are visible in the figure and the material accumulation is mainly observable after the 45° corner as the wire speed must accelerate more from the lower regulatory wire speed compared to the 60° angle. To see the results of the control strategy without such influences, the point where the speed returned to the programmed wire speed was moved another 5 mm further from the corner. A section of the modified NC code for deposition A and the 60° corner is shown in Figure 9-7.

```
N351 X21.453 Y4.254 Z12. A=0.0 B=0.0 C=0.0 RB8=0.000000 RA9=
0.000000 RL7=0.000000 ;point before the 60 degrees corner
N352 H18=8.83  ;regulatory wire speed set
;
N360 X12.273 Y-1.046 Z12. A=0.0 B=0.0 C=0.0 RB8=0.000000 RA9=
0.000000 RL7=0.000000
;
N361 X12.273 Y14.554 Z12. A=0.0 B=0.0 C=0.0 RB8=0.000000 RA9=
0.000000 RL7=0.000000 ;point after the 60 degrees corner
N362 H18=10.000  ;programmed wire speed
;
```

Figure 9-7: Section from the modified NC code

The NC codes for both deposition A and B were then executed in the control system and the 10 regulatory layers were deposited. The wire speed data were extracted from the wire feeder, to verify the set values from NC code with values from the wire feeder. The demanded speed signal is offset by 0.835 mm/s from the value in the NC code. The demanded value from the wire feeder may be the upper limit of the envelope for the wire speed signal. Figure 9-9 shows the speed values for deposition A.

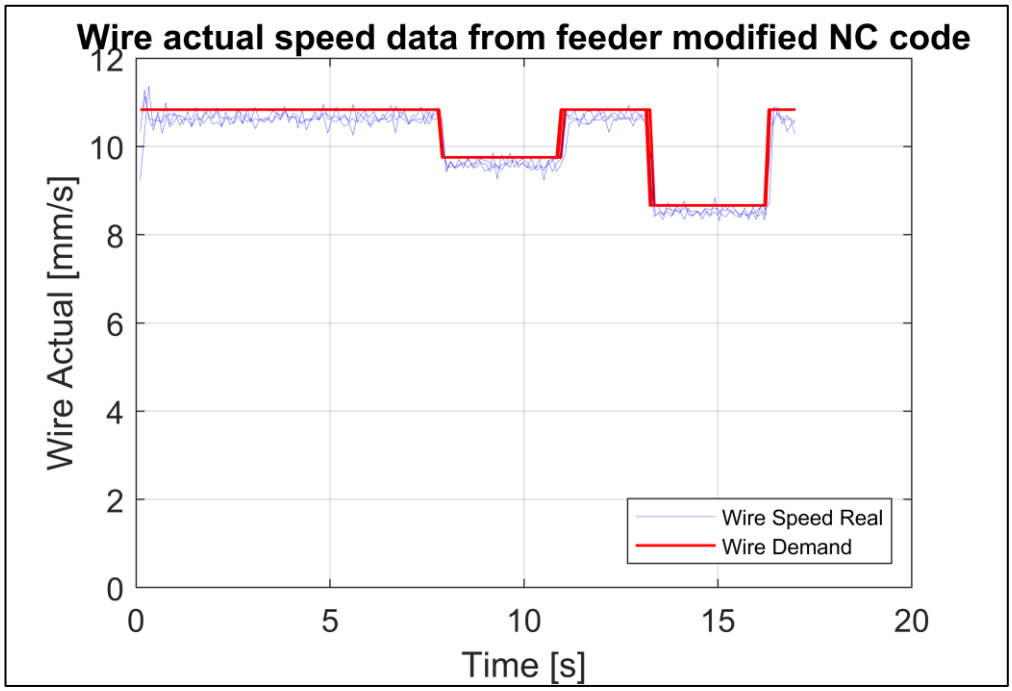

Figure 9-9: Wire speed signal from the wire feeding unit during deposition A

The 20-layer parts were then scanned again and the process of overfill detection was carried out once more. This time, the anticipated height of the part after 20 layers was set to 10.6 mm. The depositions with overfill control were then compared with a 20-layer part that had no overfill control in Figure 9-10. The unregulated deposition has a visible overfill in both the 45° and 60° corners. It is necessary to mention that the control strategy assumed consistent process conditions where the height of the layers will remain 0.53 mm. Therefore, the target height in the corner sections was 10.6 mm. However, the thermal conditions change with increasing height and deposition distance from the substrate, impacting the bead's geometry, and resulting in a lower average height of the part. This fact has been described above in Section 6. However, the control strategy targeted the height of 10.6 mm, therefore the overfill will be evaluated towards this value. Average heights of the part outside the corner sections and average heights in the vicinity of the 45° and 60° corners were also measured. A percentual difference between

the average height of the part and the height of the corners was calculated to have another comparative criterion for the control strategy validation. The results of the measurements are summarized in Table 10.

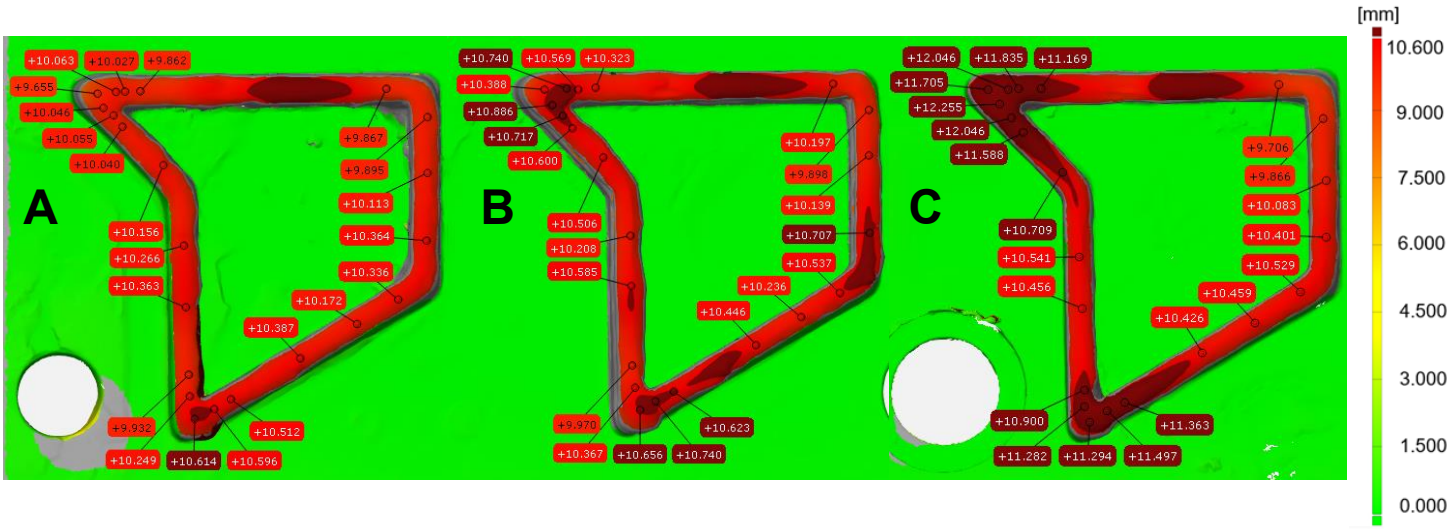

Figure 9-10: Comparison of 20-layer parts with and without an implemented control strategy

Table 10: Results of the height and overfill measurements for depositions with and without control strategy

Deposition	Overfill [mm^3]		Height [mm]		Part height [mm]	Height difference [%]	
	60°	45°	60°	45°		60°	45°
A	0.137	-	10.381	9.964	10.192	1.85	-2.24
B	1.684	1.377	10.471	10.603	10.346	1.21	2.48
C	14.571	37.572	11.267	11.806	10.317	9.21	14.43

The results show that by implementing the control strategy into the deposition process a significant reduction of material volume is achieved. The uncontrolled deposition had an overfill of 14.571 mm^3 in the 60° corner section and 37.572 mm^3 in the 45° corner section, while the parts with overfill control had an overfill of less than 1.7 mm^3. The target height of 10.6 mm was achieved in deposition B with an accuracy of ± 0.129 mm for both corner sections. Deposition A had a difference in height of -0.219 mm for the 60° corner section and -0.636 mm for the 45° corner section. However, the average height for deposition A is 0.154 mm lower than the average part height of part B and 0.125 mm lower than the average height of part C.

The height difference may be caused by greater heat accumulation during the deposition of part A compared to the other two depositions. The relatively large height difference of the 45° corner section for deposition A may be caused by overcompensation due to inaccurate evaluation of the initial overfill or due to other influences difficult to predict without temperature monitoring or overall geometrical evaluation. Outside of the overfill volumes, the percentual height difference of the corner sections towards the average part height was also improved for the parts with overfill control. The average height near the 60° corner was higher by 9.21 % compared to the average height of the part with no overfill control, for the 45° corner the height increase was 14.43 %. The maximum height difference of corner sections compared to the average part height for the parts with implemented control was 2.48 %.

The control strategy was validated by successfully regulating the overfill for the tested parts. Implementing the control strategy enhances the structural integrity of the deposition. Without it, process stability could be jeopardized due to significant offset differences between the deposition head and the part's surface throughout the deposition. The control strategy would also enable further deposition of layers by adjusting the regulatory wire speed based on the actual measured volume, considering that the overfill is already compensated by the regulatory deposition over *i* layers.

10 Conclusion and Outlook

This thesis addressed closed-loop control for a robotized LMD-w process to achieve desired structural sizes. In the first part of the theoretical section, a literature review was conducted on market-relevant metal AM technologies and their characteristics, with the findings comprehensively summarized. The second part dealt in depth with closed-loop control methods for the LMD process, detailing specific examples from existing literature. This section concluded with an overview of various sensors, controllers, controlled variables, and regulated variables used in close-loop control solutions.

In the experimental part of this work, the assumptions about material overfill in depositions, particularly in sections with sharp corners were verified. A part design including 5 different angles: 45°, 60°, 90°, 120° and 135° was used for this purpose. The overfill was observed in the vicinity of the 45° and 60° corners, caused by traverse speed dips near the corner point due to the direction change of the velocity vector and overlapping beads. The stability of the LMD-w process is highly sensitive to disturbances, therefore closed-loop control is necessary.

The system's integrated control function, which reduces wire speed based on the actual traverse speed, was activated and tested across its entire range and for multiple values of the sensitivity parameter "*k*". At k = 0.001, the function's highest sensitivity was achieved, while at k = 0.99, the function showed no activity. Nonetheless, even at the highest sensitivity setting, no improvement in overfill control was observed.

An alternative offline closed-loop control strategy, utilizing available hardware and methods was introduced. With the use of a structured light scanner, the overfill in corner sections was evaluated for 2 test parts, and the NC code was modified based on the results. The two test parts – depositions A and B were manufactured by depositing 10 layers with an experimentally verified height of 0.53 mm per layer. Overfill was identified as any height exceeding 5.3 mm, and the volumes of these overfills were measured using the established methodology. For deposition A, the overfill volumes were 14.559 mm³ and 28.816 mm³ at the 60° and 45° corners, respectively. In deposition B, these volumes were 6.216 mm³ at the 60° corner and 22.64 mm³ at the 45° corner. The distances from the corner points where the overfill began and ended were also evaluated. For deposition A both the distances for the 60° corner were 10.66 mm and 7.86 mm for the 45° corner. The length of 8.84 mm was measured for both distances of the 60°

corner for deposition B, while for the 45° corner the distance where the overfill started was 8.64 mm and the distance marking the end of the overfill was 8.06 mm. The volume and distances were key parameters for calculating the regulatory wire speed used in the modified NC code.

The control strategy was validated on both depositions A and . They were compensated by the deposition of 10 regulatory layers, where the wire speed was adjusted at defined distances before and after the corner point. For deposition A, adjusting the wire speed from 10 mm/s to 8.83 mm/s over the length of the overfill at the 60° corner and to 6.97 mm/s over the length of the overfill at the 45° corner, resulted in a measured overfill of 0.137 mm^3 at the 60° corner and no overfill was detected at the 45° corner. Moreover, the height difference was calculated as ± 2.24%, comparing the average height of the part (excluding corner areas) to the average heights measured in the vicinity of the corners. The regulatory speed values for deposition B were 9.42 mm/s for the 60° corner and 7.68 mm/s for the 45° corner, resulting in an overfill of 1.684 mm^3 and 1.377 m^3 for the 60° and 45° corners respectively. The height difference for deposition B was ≤ 2.48 % for both corners. Another 20-layer part was manufactured without the control strategy for comparison with the two test parts. The measured overfills were 14.571 mm^3 and 37.572 mm^3 for the 60° and 45° corners respectively, with the height differences being 9.21 % for the 60° corner and 14.43 for the 45° % angle. The strategy was successfully verified in reducing the overfill in corner sections and assisted in achieving desired structural sizes.

For future research, the presented closed-loop control strategy should be further developed to increase automation and achieve an online closed-loop control solution. This will require different sensors and modifications in the PLC project controlling the process. The function that is responsible for wire speed modifications should operate simultaneously with the deposition head movement to prevent undesired material accumulation. Moreover, controlling the melt pool temperature would enable a continuous deposition, eliminating the overfill caused by the starting procedure of the process, and also maintaining a constant bead geometry throughout multiple layers. Another possible solution for overfill control would to be to modify the integrated contol function either by further increasing the sensitivity to a level where wire speed can be set even lower than currently possible and by including some sort of memory to enable wire speed regulation before the actual traverse speed dip making the control more robust to control overfill not only in the area of the speed dip as this can be insufficient.

References

[1] A. Vafadar, F. Guzzomi, A. Rassau, and K. Hayward, “Advances in Metal Additive Manufacturing: A Review of Common Processes, Industrial Applications, and Current Challenges,” *Applied Sciences*, vol. 11, no. 3, Art. no. 3, Jan. 2021, doi: 10.3390/app11031213.

[2] I. Gibson, D. Rosen, B. Stucker, and M. Khorasani, *Additive Manufacturing Technologies*. Cham: Springer International Publishing, 2021. doi: 10.1007/978-3-030-56127-7.

[3] Z. Fu and C. Körner, “Actual state-of-the-art of electron beam powder bed fusion,” *European Journal of Materials*, vol. 2, no. 1, pp. 54–116, Dec. 2022, doi: 10.1080/26889277.2022.2040342.

[4] M. F. Zäh and S. Lutzmann, “Modelling and simulation of electron beam melting,” *Prod. Eng. Res. Devel.*, vol. 4, no. 1, pp. 15–23, Feb. 2010, doi: 10.1007/s11740-009-0197-6.

[5] F. Azam, A.-M. Abdul-Rani, K. Altaf, T. V. V. L. N. Rao, and H. Zaharin, “An In-Depth Review on Direct Additive Manufacturing of Metals,” *IOP Conference Series: Materials Science and Engineering*, vol. 328, p. 012005, Mar. 2018, doi: 10.1088/1757-899X/328/1/012005.

[6] M. Yakout, M. Elbestawi, and S. C. Veldhuis, “A Review of Metal Additive Manufacturing Technologies,” *Solid State Phenomena*, vol. 278, pp. 1–14, Jul. 2018, doi: 10.4028/www.scientific.net/SSP.278.1.

[7] A. Salmi, F. Calignano, M. Galati, and E. Atzeni, “An integrated design methodology for components produced by laser powder bed fusion (L-PBF) process,” *Virtual and Physical Prototyping*, vol. 13, no. 3, pp. 191–202, Jul. 2018, doi: 10.1080/17452759.2018.1442229.

[8] D.-G. Ahn, “Direct metal additive manufacturing processes and their sustainable applications for green technology: A review,” *Int. J. of Precis. Eng. and Manuf.-Green Tech.*, vol. 3, no. 4, pp. 381–395, Oct. 2016, doi: 10.1007/s40684-016-0048-9.

[9] “SLM SOLUTIONS BRINGT NEUE NXG XII 600E AUF DEN MARKT,” SLM Solutions. Accessed: Jun. 17, 2023. [Online]. Available: https://www.slm-solutions.com/de/unternehmen/news%2Draum/detail/slm%2Dsolutions%2Dbringt%2Dneue%2Dnxg%2Dxii%2D600e%2Dmit%2Derweiterter%2D15%2Dm%2Dz%2Dachse/

[10] V. B. Singh Prakash Kattire, Vinaykumar Patil, Shreyans Khot, Kiran Gujar, Rajkumar, “A review on powder bed fusion technology of metal additive manufacturing,” in *Additive Manufacturing Handbook*, CRC Press, 2017.

[11] K. Odum, L. Leung, M. Soshi, and K. Yamazaki, “Improvement of Directed Energy Deposition (DED) material addition rate via fluence-based parameter scaling method,” *Prog Addit Manuf*, vol. 7, no. 1, pp. 127–137, Feb. 2022, doi: 10.1007/s40964-021-00220-3.

[12] B. Vayre, F. Vignat, and F. Villeneuve, “Metallic additive manufacturing: State-of-the-art review and prospects,” *Mechanics & Industry*, vol. 13, pp. 89–96, Jan. 2012, doi: 10.1051/meca/2012003.

[13] J. Flores, I. Garmendia, and J. Pujana, “Toolpath generation for the manufacture of metallic components by means of the laser metal deposition technique,” *Int J Adv Manuf Technol*, vol. 101, no. 5, pp. 2111–2120, Apr. 2019, doi: 10.1007/s00170-018-3124-1.

[14] Y. Ding, R. Dwivedi, and R. Kovacevic, “Process planning for 8-axis robotized laser-based direct metal deposition system: A case on building revolved part,” *Robotics and Computer-Integrated Manufacturing*, vol. 44, pp. 67–76, Apr. 2017, doi: 10.1016/j.rcim.2016.08.008.

[15] M. Manoharan and S. Kumaraguru, “Novel process planning approach for support-free additive manufacturing using multi-axis deposition systems,” *International Journal of Computer Integrated Manufacturing*, vol. 36, no. 6, pp. 807–829, Jun. 2023, doi: 10.1080/0951192X.2022.2145020.

[16] D.-G. Ahn, “Directed Energy Deposition (DED) Process: State of the Art,” *Int. J. of Precis. Eng. and Manuf.-Green Tech.*, vol. 8, no. 2, Art. no. 2, Mar. 2021, doi: 10.1007/s40684-020-00302-7.

[17] S. P. Kumar, S. Elangovan, R. Mohanraj, and B. Srihari, “Critical review of off-axial nozzle and coaxial nozzle for powder metal deposition,” *Materials Today: Proceedings*, vol. 46, pp. 8066–8079, Jan. 2021, doi: 10.1016/j.matpr.2021.03.037.

[18] A. Bandyopadhyay, Y. Zhang, and S. Bose, “Recent developments in metal additive manufacturing,” *Current Opinion in Chemical Engineering*, vol. 28, pp. 96–104, Jun. 2020, doi: 10.1016/j.coche.2020.03.001.

[19] J.-S. Lim, W.-J. Oh, C.-M. Lee, and D.-H. Kim, “Selection of effective manufacturing conditions for directed energy deposition process using machine learning methods,” *Sci Rep*, vol. 11, no. 1, Art. no. 1, Dec. 2021, doi: 10.1038/s41598-021-03622-z.

[20] S. Nowotny, S. Thieme, D. Albert, F. Kubisch, R. Kager, and C. Leyens, “Generative Manufacturing and Repair of Metal Parts through Direct Laser Deposition Using Wire Material,” in *Digital Product and Process Development Systems*, vol. 411, G. L. Kovács and D. Kochan, Eds., in IFIP Advances in Information and Communication Technology, vol. 411. , Berlin, Heidelberg: Springer Berlin Heidelberg, 2013, pp. 185–189. doi: 10.1007/978-3-642-41329-2_20.

[21] T. DebRoy *et al.*, “Additive manufacturing of metallic components – Process, structure and properties,” *Progress in Materials Science*, vol. 92, pp. 112–224, Mar. 2018, doi: 10.1016/j.pmatsci.2017.10.001.

[22] R. M. Mahamood and E. T. Akinlabi, “Processing Parameters Optimization for Material Deposition Efficiency in Laser Metal Deposited Titanium Alloy,” *Lasers Manuf. Mater. Process.*, vol. 3, no. 1, Art. no. 1, Mar. 2016, doi: 10.1007/s40516-015-0020-5.

[23] E. Brandl, F. Palm, V. Michailov, B. Viehweger, and C. Leyens, “Mechanical properties of additive manufactured titanium (Ti–6Al–4V) blocks deposited by a solid-state laser and wire,” *Materials & Design*, vol. 32, no. 10, Art. no. 10, Dec. 2011, doi: 10.1016/j.matdes.2011.06.062.

[24] L. Wang, J. Xue, and Q. Wang, “Correlation between arc mode, microstructure, and mechanical properties during wire arc additive manufacturing of 316L stainless steel,” *Materials Science and Engineering: A*, vol. 751, pp. 183–190, Mar. 2019, doi: 10.1016/j.msea.2019.02.078.

[25] S. Negi *et al.*, “Review on electron beam based additive manufacturing,” *Rapid Prototyping Journal*, vol. 26, no. 3, pp. 485–498, Jan. 2019, doi: 10.1108/RPJ-07-2019-0182.

[26] K. Taminger and R. Hafley, “Electron Beam Freeform Fabrication: A Rapid Metal Deposition Process,” Jul. 2003. Accessed: Jan. 04, 2023. [Online]. Available: https://www.semanticscholar.org/paper/Electron-Beam-Freeform-Fabrication%3A-A-Rapid-Metal-Taminger-Hafley/a53cfe41eb209eb904c089c04b83131581e186cf

[27] “Sciaky.” Accessed: Jan. 04, 2023. [Online]. Available: https://www.sciaky.com/additive-manufacturing/wire-vs-powder

[28] D. Ding, Z. Pan, D. Cuiuri, and H. Li, “Wire-feed additive manufacturing of metal components: technologies, developments and future interests,” *Int J Adv Manuf Technol*, vol. 81, no. 1, pp. 465–481, Oct. 2015, doi: 10.1007/s00170-015-7077-3.

[29] K. M. Taminger and R. A. Hafley, “Electron Beam Freeform Fabrication for Cost Effective Near-Net Shape Manufacturing,” presented at the NATO/RTO AVT-139 Specialists’’ Meeting on Cost Effective Manufacture via Net Shape Processing, Amsterdam, May 2006. Accessed: Jan. 04, 2023. [Online]. Available: https://ntrs.nasa.gov/citations/20080013538

[30] E. Soylemez, J. Beuth, and K. Taminger, “Controlling melt pool dimensions over a wide range of material deposition rates in electron beam additive manufacturing,” presented at the 21st Annual International Solid Freeform Fabrication Symposium - An Additive Manufacturing Conference, SFF 2010, Jan. 2010.

[31] T. A. Rodrigues, V. Duarte, R. M. Miranda, T. G. Santos, and J. P. Oliveira, “Current Status and Perspectives on Wire and Arc Additive Manufacturing (WAAM),” *Materials*, vol. 12, no. 7, Art. no. 7, Jan. 2019, doi: 10.3390/ma12071121.

[32] B. Wu *et al.*, “A review of the wire arc additive manufacturing of metals: properties, defects and quality improvement,” *Journal of Manufacturing Processes*, vol. 35, pp. 127–139, Oct. 2018, doi: 10.1016/j.jmapro.2018.08.001.

[33] N. Rodriguez, L. Vázquez, I. Huarte, E. Arruti, I. Tabernero, and P. Alvarez, “Wire and arc additive manufacturing: a comparison between CMT and TopTIG processes applied to stainless steel,” *Weld World*, vol. 62, no. 5, pp. 1083–1096, Sep. 2018, doi: 10.1007/s40194-018-0606-6.

[34] A. R. McAndrew *et al.*, “Interpass rolling of Ti-6Al-4V wire + arc additively manufactured features for microstructural refinement,” *Additive Manufacturing*, vol. 21, pp. 340–349, May 2018, doi: 10.1016/j.addma.2018.03.006.

[35] C. M. A. Silva, I. M. F. Bragança, A. Cabrita, L. Quintino, and P. A. F. Martins, “Formability of a wire arc deposited aluminium alloy,” *J Braz. Soc. Mech. Sci. Eng.*, vol. 39, no. 10, Art. no. 10, Oct. 2017, doi: 10.1007/s40430-017-0864-z.

[36] J. Ding *et al.*, “Thermo-mechanical analysis of Wire and Arc Additive Layer Manufacturing process on large multi-layer parts,” *Computational Materials Science*, vol. 50, no. 12, pp. 3315–3322, Dec. 2011, doi: 10.1016/j.commatsci.2011.06.023.

[37] I. Garmendia, J. Pujana, A. Lamikiz, M. Madarieta, and J. Leunda, “Structured light-based height control for laser metal deposition,” *Journal of Manufacturing Processes*, vol. 42, pp. 20–27, Jun. 2019, doi: 10.1016/j.jmapro.2019.04.018.

[38] T. Mukherjee and T. DebRoy, “A digital twin for rapid qualification of 3D printed metallic components,” *Applied Materials Today*, vol. 14, pp. 59–65, Mar. 2019, doi: 10.1016/j.apmt.2018.11.003.

[39] C. Stehmar, M. Gipperich, M. Kogel-Hollacher, A. Velazquez Iturbide, and R. H. Schmitt, “Inline Optical Coherence Tomography for Multidirectional Process Monitoring in a Coaxial LMD-w Process,” *Applied Sciences*, vol. 12, no. 5, Art. no. 5, Jan. 2022, doi: 10.3390/app12052701.

[40] Y. Chen *et al.*, “Coaxial laser metal wire deposition of Ti6Al4V alloy: process, microstructure and mechanical properties,” *Journal of Materials Research and Technology*, vol. 20, pp. 2578–2590, Sep. 2022, doi: 10.1016/j.jmrt.2022.08.068.

[41] “Additive production|Laser deposition welding | PRECITEC.” Accessed: Jan. 04, 2024. [Online]. Available: https://www.precitec.com/laser-welding/products/processing-heads/coax-printer/

[42] S. Ji, F. Liu, T. Shi, G. Fu, and S. Shi, “Effects of Defocus Distance on Three-Beam Laser Internal Coaxial Wire Cladding,” *Chinese Journal of Mechanical Engineering*, vol. 34, no. 1, p. 45, May 2021, doi: 10.1186/s10033-021-00560-9.

[43] "Coaxial laser wire cladding head COAXwire - Fraunhofer IWS," Fraunhofer Institute for Material and Beam Technology IWS. Accessed: Jun. 17, 2023. [Online]. Available: https://www.iws.fraunhofer.de/en/technologyfields/additive-manufacturing-and-surface-technologies/laser_cladding/system_technology/COAXwire.html

[44] "Coaxial laser wire processing optic COAXwire mini - Fraunhofer IWS," Fraunhofer Institute for Material and Beam Technology IWS. Accessed: Jun. 17, 2023. [Online]. Available: https://www.iws.fraunhofer.de/en/technologyfields/additive-manufacturing-and-surface-technologies/laser_cladding/system_technology/COAXwire_mini.html

[45] M. Roberts, M. Xia, and A. Kennedy, "Data-driven Process Parameter Optimisation for Laser Wire Metal Additive Manufacturing," in *2022 27th International Conference on Automation and Computing (ICAC)*, Sep. 2022, pp. 1–6. doi: 10.1109/ICAC55051.2022.9911139.

[46] "Brochure_Meltio_M450_August2022_E-1.pdf." Accessed: Jun. 17, 2023. [Online]. Available: https://meltio3d.com/wp-content/uploads/2022/10/Brochure_Meltio_M450_August2022_E-1.pdf

[47] "Meltio Partners With 12 Leading Software Companies To Foster Hybrid And Robotic AM Adoption - Manufactur3D." Accessed: Jun. 17, 2023. [Online]. Available: https://manufactur3dmag.com/meltio-leading-software-companies-am-adoption/

[48] M. Motta, A. G. Demir, and B. Previtali, "High-speed imaging and process characterization of coaxial laser metal wire deposition," *Additive Manufacturing*, vol. 22, pp. 497–507, Aug. 2018, doi: 10.1016/j.addma.2018.05.043.

[49] P. Singh and D. Dutta, "Multi-Direction Layered Deposition – An Overview of Process Planning Methodologies," *Proceedings of the Solid Freeform Fabrication Symposium*, Jan. 2003.

[50] D. Jafari, T. H. J. Vaneker, and I. Gibson, "Wire and arc additive manufacturing: Opportunities and challenges to control the quality and accuracy of manufactured parts," *Materials & Design*, vol. 202, p. 109471, Apr. 2021, doi: 10.1016/j.matdes.2021.109471.

[51] L. Yang *et al.*, *Additive Manufacturing of Metals: The Technology, Materials, Design and Production*. in Springer Series in Advanced Manufacturing. Cham: Springer International Publishing, 2017. doi: 10.1007/978-3-319-55128-9.

[52] M. Akbari, Y. Ding, and R. Kovacevic, "Process Development for a Robotized Laser Wire Additive Manufacturing," in *Volume 2: Additive Manufacturing; Materials*, Los Angeles, California, USA: American Society of Mechanical Engineers, Jun. 2017, p. V002T01A015. doi: 10.1115/MSEC2017-2951.

[53] M. Akbari and R. Kovacevic, "Closed loop control of melt pool width in robotized laser powder–directed energy deposition process," *Int J Adv Manuf Technol*, vol. 104, no. 5, pp. 2887–2898, Oct. 2019, doi: 10.1007/s00170-019-04195-y.

[54] C. J. Bernauer, A. Zapata, L. Kick, T. Weiss, M. E. Sigl, and M. F. Zaeh, "Pyrometry-based closed-loop control of the melt pool temperature in Laser Metal Deposition with coaxial wire feeding," *Procedia CIRP*, vol. 111, pp. 296–301, Jan. 2022, doi: 10.1016/j.procir.2022.08.025.

[55] L. Tang and R. G. Landers, "Melt Pool Temperature Control for Laser Metal Deposition Processes—Part II: Layer-to-Layer Temperature Control," *Journal of Manufacturing Science and Engineering*, vol. 132, no. 011011, Jan. 2010, doi: 10.1115/1.4000883.

[56] D. Salehi and M. Brandt, "Melt pool temperature control using LabVIEW in Nd:YAG laser blown powder cladding process," *Int J Adv Manuf Technol*, vol. 29, no. 3, pp. 273–278, Jun. 2006, doi: 10.1007/s00170-005-2514-3.

[57] N. Pirch *et al.*, "Temperature field and residual stress distribution for laser metal deposition," *Journal of Laser Applications*, vol. 30, no. 3, p. 032503, Jun. 2018, doi: 10.2351/1.5040634.

[58] L. Tang and R. G. Landers, "Melt Pool Temperature Control for Laser Metal Deposition Processes—Part I: Online Temperature Control," *Journal of Manufacturing Science and Engineering*, vol. 132, no. 011010, Jan. 2010, doi: 10.1115/1.4000882.

[59] G. Bi, A. Gasser, K. Wissenbach, A. Drenker, and R. Poprawe, "Identification and qualification of temperature signal for monitoring and control in laser cladding," *Optics and Lasers in Engineering*, vol. 44, no. 12, pp. 1348–1359, Dec. 2006, doi: 10.1016/j.optlaseng.2006.01.009.

[60] V. L. D. S. N. Button, "Chapter 4 - Temperature Transducers," in *Principles of Measurement and Transduction of Biomedical Variables*, V. L. D. S. N. Button, Ed., Oxford: Academic Press, 2015, pp. 101–154. doi: 10.1016/B978-0-12-800774-7.00004-0.

[61] R. Hathaway and K. W. Long, "1 - TRANSDUCERS AND DATA ACQUISITION," in *Fatigue Testing and Analysis*, Y.-L. Lee, J. Pan, R. B. Hathaway, and M. E. Barkey, Eds., Burlington: Butterworth-Heinemann, 2005, pp. 1–56. doi: 10.1016/B978-075067719-6/50002-6.

[62] J. P. Bentley, *Principles of measurement systems*. Harlow, England ; New York : Pearson Prentice Hall, 2005. Accessed: Dec. 30, 2023. [Online]. Available: http://archive.org/details/principlesofmeas0000bent_y4c1

[63] B. Gerardus Richardus Römer, "Modelling and control of laser surface treatment," Jun. 1999, Accessed: Jun. 19, 2023. [Online]. Available: https://research.utwente.nl/en/publications/modelling-and-control-of-laser-surface-treatment

[64] M. L. Griffith *et al.*, "Understanding thermal behavior in the LENS process," *Materials & Design*, vol. 20, no. 2, pp. 107–113, Jun. 1999, doi: 10.1016/S0261-3069(99)00016-3.

[65] S. Barua, F. Liou, J. Newkirk, and T. Sparks, "Vision-based defect detection in laser metal deposition process," *Rapid Prototyping Journal*, vol. 20, no. 1, pp. 77–85, Jan. 2014, doi: 10.1108/RPJ-04-2012-0036.

[66] M. H. Farshidianfar, A. Khajepour, and A. Gerlich, "Real-time control of microstructure in laser additive manufacturing," *Int J Adv Manuf Technol*, vol. 82, no. 5, pp. 1173–1186, Feb. 2016, doi: 10.1007/s00170-015-7423-5.

[67] G. Bi, A. Gasser, K. Wissenbach, A. Drenker, and R. Poprawe, "Characterization of the process control for the direct laser metallic powder deposition," *Surface and Coatings Technology*, vol. 201, no. 6, pp. 2676–2683, Dec. 2006, doi: 10.1016/j.surfcoat.2006.05.006.

[68] Z. jue Tang *et al.*, "A review on in situ monitoring technology for directed energy deposition of metals," *International Journal of Advanced Manufacturing Technology*, vol. 108, no. 11–12, pp. 3437–3463, Jun. 2020, doi: 10.1007/s00170-020-05569-3.

[69] L. Miao, F. Xing, and Y. Chai, "Closed Loop Control of Melt Pool Width in Laser Directed Energy Deposition Process Based on PSO-LQR," *IEEE Access*, vol. 11, pp. 78170–78181, 2023, doi: 10.1109/ACCESS.2023.3292789.

[70] B. T. Gibson *et al.*, "Melt pool size control through multiple closed-loop modalities in laser-wire directed energy deposition of Ti-6Al-4V," *Additive Manufacturing*, vol. 32, p. 100993, Mar. 2020, doi: 10.1016/j.addma.2019.100993.

[71] J. Rodriguez-Araujo, J. J. Rodriguez-andina, J. Farina, F. Vidal, J. L. Mato, and M. A. Montealegre, "Industrial Laser Cladding Systems: FPGA-Based Adaptive Control," *IEEE*

Industrial Electronics Magazine, vol. 6, no. 4, pp. 35–46, Dec. 2012, doi: 10.1109/MIE.2012.2221356.

[72] D. Hu and R. Kovacevic, "Modelling and measuring the thermal behaviour of the molten pool in closed-loop controlled laser-based additive manufacturing," *Proceedings of the Institution of Mechanical Engineers, Part B: Journal of Engineering Manufacture*, vol. 217, no. 4, pp. 441–452, 2003, doi: 10.1243/095440503321628125.

[73] E. Toyserkani, A. Khajepour, and S. F. Corbin, "Control of Laser Cladding Process," in *Laser Cladding*, CRC Press, 2004.

[74] D. Regulin and R. Barucci, "A benchmark of approaches for closed loop control of melt pool shape in DED," *Int J Adv Manuf Technol*, vol. 126, no. 1, pp. 829–843, May 2023, doi: 10.1007/s00170-023-11042-8.

[75] M. Akbari and R. Kovacevic, "An investigation on mechanical and microstructural properties of 316LSi parts fabricated by a robotized laser/wire direct metal deposition system," *Additive Manufacturing*, vol. 23, pp. 487–497, Oct. 2018, doi: 10.1016/j.addma.2018.08.031.

[76] J. T. Hofman, B. Pathiraj, J. van Dijk, D. F. de Lange, and J. Meijer, "A camera based feedback control strategy for the laser cladding process," *Journal of Materials Processing Technology*, vol. 212, no. 11, pp. 2455–2462, Nov. 2012, doi: 10.1016/j.jmatprotec.2012.06.027.

[77] D. Thakkar and H. Sahasrabudhe, "Investigating microstructure and defects evolution in laser deposited single-walled Ti6Al4V structures with sharp and non-sharp features," *Journal of Manufacturing Processes*, vol. 56, pp. 928–940, Aug. 2020, doi: 10.1016/j.jmapro.2020.05.052.

[78] A. Zapata, C. Bernauer, C. Stadter, C. G. Kolb, and M. F. Zaeh, "Investigation on the Cause-Effect Relationships between the Process Parameters and the Resulting Geometric Properties for Wire-Based Coaxial Laser Metal Deposition," *Metals*, vol. 12, no. 3, Art. no. 3, Mar. 2022, doi: 10.3390/met12030455.

[79] D. Montoya-Zapata *et al.*, "Computational minimization of over-deposition at corners of trajectories in Laser Metal Deposition," *Manufacturing Letters*, vol. 29, pp. 29–33, Aug. 2021, doi: 10.1016/j.mfglet.2021.05.001.

[80] J. C. Pereira, H. Borovkov, F. Zubiri, M. C. Guerra, and J. Caminos, "Optimization of Thin Walls with Sharp Corners in SS316L and IN718 Alloys Manufactured with Laser Metal Deposition," *JMMP*, vol. 5, no. 1, p. 5, Jan. 2021, doi: 10.3390/jmmp5010005.

[81] A. Zapata *et al.*, "A model-based approach to reduce kinematics-related overfill in robot-guided Laser Directed Energy Deposition," *CIRP Journal of Manufacturing Science and Technology*, vol. 45, pp. 200–209, Oct. 2023, doi: 10.1016/j.cirpj.2023.06.014.

[82] D. Knüttel, S. Baraldo, A. Valente, F. Bleicher, K. Wegener, and E. Carpanzano, "Machine learning based track height prediction for complex tool paths in direct metal deposition," *CIRP Annals*, vol. 71, May 2022, doi: 10.1016/j.cirp.2022.03.032.

[83] O. Nenadl, V. Ocelík, A. Palavra, and J. Th. M. D. Hosson, "The Prediction of Coating Geometry from Main Processing Parameters in Laser Cladding," *Physics Procedia*, vol. 56, pp. 220–227, Jan. 2014, doi: 10.1016/j.phpro.2014.08.166.

[84] Y.-Y. Woo, S.-W. Han, I.-Y. Oh, Y.-H. Moon, and W. Ha, "Control of Directed Energy Deposition Process to Obtain Equal-Height Rectangular Corner," *Int. J. Precis. Eng. Manuf.*, vol. 20, no. 12, pp. 2129–2139, Dec. 2019, doi: 10.1007/s12541-019-00226-6.

[85] J. I. Arrizubieta, S. Martínez, A. Lamikiz, E. Ukar, K. Arntz, and F. Klocke, "Instantaneous powder flux regulation system for Laser Metal Deposition," *Journal of*

Manufacturing Processes, vol. 29, pp. 242–251, Oct. 2017, doi: 10.1016/j.jmapro.2017.07.018.

[86] A. Fathi, A. Khajepour, E. Toyserkani, and M. Durali, "Clad height control in laser solid freeform fabrication using a feedforward PID controller," *Int J Adv Manuf Technol*, vol. 35, no. 3, pp. 280–292, Dec. 2007, doi: 10.1007/s00170-006-0721-1.

[87] T. Shi, J. Shi, Z. Xia, B. Lu, S. Shi, and G. Fu, "Precise control of variable-height laser metal deposition using a height memory strategy," *Journal of Manufacturing Processes*, vol. 57, pp. 222–232, Sep. 2020, doi: 10.1016/j.jmapro.2020.05.026.

[88] Y. Hua and J. Choi, "Adaptive direct metal/material deposition process using a fuzzy logic-based controller," *Journal of Laser Applications*, vol. 17, no. 4, pp. 200–210, Nov. 2005, doi: 10.2351/1.2098811.

[89] A. Heralić, A.-K. Christiansson, and B. Lennartson, "Height control of laser metal-wire deposition based on iterative learning control and 3D scanning," *Optics and Lasers in Engineering*, vol. 50, no. 9, pp. 1230–1241, Sep. 2012, doi: 10.1016/j.optlaseng.2012.03.016.

[90] S. Takushima, D. Morita, N. Shinohara, H. Kawano, Y. Mizutani, and Y. Takaya, "Optical in-process height measurement system for process control of laser metal-wire deposition," *Precision Engineering*, vol. 62, pp. 23–29, Mar. 2020, doi: 10.1016/j.precisioneng.2019.11.007.

[91] C. Bernauer *et al.*, "Segmentation-based closed-loop layer height control for enhancing stability and dimensional accuracy in wire-based laser metal deposition," *Robotics and Computer-Integrated Manufacturing*, vol. 86, p. 102683, Apr. 2024, doi: 10.1016/j.rcim.2023.102683.

[92] L. Song, V. Bagavath-Singh, B. Dutta, and J. Mazumder, "Control of melt pool temperature and deposition height during direct metal deposition process," *Int J Adv Manuf Technol*, vol. 58, no. 1, pp. 247–256, Jan. 2012, doi: 10.1007/s00170-011-3395-2.

[93] L. Tang and R. G. Landers, "Layer-to-Layer Height Control for Laser Metal Deposition Process," *Journal of Manufacturing Science and Engineering*, vol. 133, no. 2, p. 021009, Apr. 2011, doi: 10.1115/1.4003691.

[94] D. Becker *et al.*, "Influence of a closed-loop controlled laser metal wire deposition process of S Al 5356 on the quality of manufactured parts before and after subsequent machining," *Prod. Eng. Res. Devel.*, vol. 15, no. 3, pp. 489–507, Jun. 2021, doi: 10.1007/s11740-021-01030-w.

[95] A. Heralić, A.-K. Christiansson, M. Ottosson, and B. Lennartson, "Increased stability in laser metal wire deposition through feedback from optical measurements," *Optics and Lasers in Engineering*, vol. 48, no. 4, pp. 478–485, Apr. 2010, doi: 10.1016/j.optlaseng.2009.08.012.

[96] J. E. Bobrow, S. Dubowsky, and J. S. Gibson, "Time-Optimal Control of Robotic Manipulators Along Specified Paths," *The International Journal of Robotics Research*, vol. 4, no. 3, pp. 3–17, Sep. 1985, doi: 10.1177/027836498500400301.

[97] A. Donges and R. Noll, "Optical Coherence Tomography: OCT," in *Laser Measurement Technology: Fundamentals and Applications*, A. Donges and R. Noll, Eds., in Springer Series in Optical Sciences. , Berlin, Heidelberg: Springer, 2015, pp. 227–245. doi: 10.1007/978-3-662-43634-9_9.

[98] C. Stadter, M. Schmoeller, M. Zeitler, V. Tueretkan, U. Munzert, and M. F. Zaeh, "Process control and quality assurance in remote laser beam welding by optical coherence tomography," *Journal of Laser Applications*, vol. 31, no. 2, p. 022408, Apr. 2019, doi: 10.2351/1.5096103.

[99] S. A. Morgan *et al.*, “Real-time process control in CO2 laser welding and direct casting: Focus and temperature,” in *International Congress on Applications of Lasers & Electro-Optics*, San Diego, California, USA: Laser Institute of America, 1997, pp. G290–G299. doi: 10.2351/1.5059735.

[100] “OK Autrod 316LSi,” EUROPE ENGLISH. Accessed: Dec. 05, 2023. [Online]. Available: https://esab.com/gs/eur_en/products-solutions/product/filler-metals/stainless-steel/mig-wires-tig-rods-gmaw-gtaw/ok-autrod-316lsi/

[101] “1.4301 | AISI 304 | Nerezová ocel | AGST Drát,” agst. Accessed: Jan. 01, 2024. [Online]. Available: https://www.agst.de/4301?lang=cs

[102] Martin Novák, “Robot control to ensure quality welding technology,” Czech Technical University in Prague, Prague, 2022. [Online]. Available: https://dspace.cvut.cz/bitstream/handle/10467/103511/F2-DP-2022-Novak-Martin-DP-Novak_kos.pdf?sequence=-1&isAllowed=y

[103] “Sensors | Free Full-Text | Absolute Positioning Accuracy Improvement in an Industrial Robot.” Accessed: Dec. 27, 2023. [Online]. Available: https://www.mdpi.com/1424-8220/20/16/4354

[104] S. He, C. Yan, Y. Deng, C.-H. Lee, and X. Zhou, “A tolerance constrained G2 continuous path smoothing and interpolation method for industrial SCARA robots,” *Robotics and Computer-Integrated Manufacturing*, vol. 63, p. 101907, Jun. 2020, doi: 10.1016/j.rcim.2019.101907.

List of Figures

List of Tables

List of Used Software

1. MATLAB R2023b
2. Siemens NX 2306
3. Autodesk Inventor Professional 2024
4. Autodesk Fusion 360
5. Atos Professional Software 2018